European Journal of Medicinal Chemistry 143 (2018) 983–996

Contents lists available at ScienceDirect

European Journal of Medicinal Chemistry

journal homepage: http://www.elsevier.com/locate/ejmech

Research paper

Bioactive products from singlet oxygen photooxygenation of cannabinoids

Ahmed Galal Osman [a, *], Khaled M. Elokely [b, c, d], Vivek K. Yadav [b, c], Paulo Carvalho [e], Mohamed Radwan [a], Desmond Slade [f], Waseem Gul [a, g], Shabana Khan [a, h], Olivia R. Dale [a], Afeef S. Husni [h], Michael L. Klein [b, c], Stephen J. Cutler [h, 1], Samir A. Ross [a, h], Mahmoud A. ElSohly [g, i, **]

[a] National Center for Natural Products Research, The University of Mississippi, University, MS 38677, United States
[b] Institute for Computational Molecular Science, Temple University, Philadelphia, PA 19122, United States
[c] Department of Chemistry, Temple University, Philadelphia, PA 19122, United States
[d] Department of Pharmaceutical Chemistry, Tanta University, Tanta 31527, Egypt
[e] Feik School of Pharmacy, University of the Incarnate Word, San Antonio, TX 78209, United States
[f] MRI Global, 425 Volker Boulevard, Kansas City, MO, United States
[g] ElSohly Laboratories, Inc., 5 Industrial Park Drive, Oxford, MS 38655, United States
[h] Department of of BioMolecular Sciences, University of Mississippi, University, MS 38677, United States
[i] Department of Pharmaceutics, University of Mississippi, University, MS 38677, United States

ARTICLE INFO

Article history:
Received 5 July 2017
Received in revised form
14 October 2017
Accepted 17 November 2017
Available online 21 November 2017

Keywords:
Cannabinoids
Photooxygenation
CB_1 agonists
Antimicrobial
Anticancer
Antileishmanial

ABSTRACT

Photooxygenation of Δ^8 tetrahydrocannabinol (Δ^8-THC), Δ^9 tetrahydrocannabinol (Δ^9-THC), Δ^9 tetrahydrocannabinolic acid (Δ^9-THCA) and some derivatives (acetate, tosylate and methyl ether) yielded 24 oxygenated derivatives, 18 of which were new and 6 were previously reported, including allyl alcohols, ethers, quinones, hydroperoxides, and epoxides. Testing these compounds for their modulatory effect on cannabinoid receptors CB_1 and CB_2 led to the identification of **7** and **21** as CB_1 partial agonists with Ki values of 0.043 μM and 0.048 μM, respectively and **23** as a cannabinoid with high binding affinity for CB_2 with Ki value of 0.0095 μM, but much less affinity towards CB_1 (Ki 0.467 μM). The synthesized compounds showed cytotoxic activity against cancer cell lines (SK-MEL, KB, BT-549, and SK-OV-3) with IC_{50} values ranging from 4.2 to 8.5 μg/mL. Several of those compounds showed antimicrobial, antimalarial and antileishmanial activities, with compound **14** being the most potent against various pathogens.

1. Introduction

Cannabinoids, from *Cannabis sativa* L., have been the focus of extensive chemical and biological research due to their unique behavioral, psychotropic and other pharmacological effects. The discovery that some of their biological activities could be translated into treatments for a number of serious illnesses, such as glaucoma, depression, neuralgia, multiple sclerosis, Alzheimer's disease, alleviation of symptoms of HIV/AIDS and cancer [1–4] has given momentum for further exploration of their chemical and biological properties. The discovery of cannabinoid receptors CB_1 and CB_2 (with other possible receptors currently under investigation) [5,6] opened new possibilities for the design and exploration of cannabinoid structures. CB_1 agonists exhibit analgesic properties, whereas CB_1 antagonists and inverse agonists have shown the potential to act as therapeutic agents against diabetes, drug dependence, and obesity. CB_2 agonists have exhibited cytotoxicity and demonstrated potential for treatment of neuropathic pain [7–9], suppression of inflammation [10] and attenuation of the severity of disease in animal models of multiple sclerosis [11] and age-related illnesses [12–14].

In search of compounds with affinity for CB_1 and CB_2 cannabinoid receptors our group decided to explore preparation and

* Corresponding author.
** Corresponding author. ElSohly Laboratories, Inc., 5 Industrial Park Drive, Oxford, MS 38655, United States.
E-mail address: amgalalv@yahoo.com (A. Galal Osman).
[1] Current affiliation: University of South Carolina College of Pharmacy, Columbia, SC 29208.

https://doi.org/10.1016/j.ejmech.2017.11.043
0223-5234/

testing oxygenated derivatives of Δ^9-THC and its isomer Δ^8-THC through photooxygenation. One of the earliest references reporting the photooxygenation of Δ^8-THC acetate via irradiation with UV light in the presence of oxygen and using rose bengal as a photosensitizer [15] yielded three hydroperoxides: (−)-8α- and (−)-8β-hydroperoxido-$\Delta^{9,11}$-THC acetate, and (−)-9α-hydroperoxido-$\Delta^{7,8}$-THC acetate. More recently, other oxygenated derivatives of Δ^9-THC and Δ^8-THC have been prepared and showed antibacterial [16] and anticancer effects [17–20], as well as demonstrating some degree of affinity to cannabinoid receptors CB_1 and CB_2 [21,22].

This article is a continuation of our previous work [23] and describes the photooxygenation of Δ^9-tetrahydrocannabinol (Δ^9-THC - **1**), Δ^8-tetrahydrocannabinol (Δ^8-THC - **2**), Δ^9-tetrahydrocannabinolic acid (Δ^9-THCA - **8**) and some of their derivatives (Fig. 1) under different conditions. *Meso*-tetraphenylporphine was used as a photosensitizer in presence of oxygen and irradiation with incandescent light, generating singlet oxygen ($^1O_2$*), which reacted with the trisubstituted olefinic moiety to form oxygenated products. Six of those compounds (**15, 23, 10, 12, 14** and **31**) have been previously reported as minor oxygenated cannabinoids from cannabis, serum metabolites of Δ^9-THC, or products from non-photooxygenation reactions [15,24–29].

These compounds were screened for various biological activities, including antimicrobial (*Staphylococcus aureus*, methicillin-resistant *Staphylococcus aureus* [MRSA]), antifungal (*Cryptococcus neoformans*, *Candida glabrata*, and *Candida krusei*), anticancer (cell lines SK-MEL, KB, BT-549, and SK-OV-3), antimalarial (*Plasmodium falciparum*, D6 clone - chloroquine-sensitive - and W2 clone - chloroquine-resistant) and antileishmanial (*Leishmania major*), as well as their binding affinity towards cannabinoid receptors CB_1 and CB_2.

2. Results and discussion

2.1. Chemistry

Photooxygenation of **1**, **2**, tosylates **3** and **4** [25], methoxy-Δ^8-THC **5**, Δ^9-THC acetate **6**, Δ^8-THC acetate **7,** and Δ^9-THCA **8** using *meso*-tetraphenylporphine as a photosensitizer [30] resulted in the formation of 24 derivatives. Six of them (**15, 23, 10, 12, 14** and **31**) have been previously reported [15,24–29] and the other 18 are, to the best of our knowledge, novel compounds. One of our goals was to generate a large array of oxygenated derivatives in order to correlate the position and nature of those functionalities with their biological activity. Initial studies revealed that changes in polarity of the reactional solvent system led to the formation of products with different patterns of oxygenation, and this knowledge was used to guide the choice of solvents with variable polarities for our reactions. Reaction conditions and corresponding products are summarized on Table 1.

Some of the products were subjected to further treatment under different conditions. Compound **18**, submitted to reduction with dimethyl sulfide for 22 h, yielded the allylic alcohol **19** (Scheme 2); epoxide **27**, reduced with $NaBH_4$ or $NaHCO_3/H_2O$/Adogen 464, afforded compound **29**, while reduction with Pd/C yielded compound **30** (Scheme 5). Attempted reduction of compounds **21**, **22** and hydroperoxides **24**, **25**, resulted in decomposition. Alkaline hydrolysis of **21** yielded the known tertiary allylic alcohol **23** (Scheme 3), while attempted hydrolysis of **22** resulted also in decomposition.

X-ray analysis of compound **20** [31] (CCDC reference: 1442416), crystallized from ethyl acetate: hexanes 1:9 producing needle-like crystals, allowed for confirmation of structure and the establishment of its relative configuration (Fig. 2).

Compounds **25** and **26** (Scheme 4) were obtained as separated compounds and exhibited different chromatographic behavior on TLC, R_f = 0.42 (Hexanes- DCM-MeOH, 9:9:0.8) and R_f = 0.36 (Hexanes - DCM-MeOH, 9:9:0.8) respectively. They also display different specific rotation values and different ^1H and ^{13}C NMR shifts. However, none of the spectroscopic methods used was capable of assigning with certainty the configuration of each isomer and we were unable to obtain a crystalline sample for X-ray analysis.

2.2. Stereochemical assignments

Stereochemical assignments for derivatives **9**, **13**, **17**, **18**, **19, 21**, **24** were determined on the basis of NOESY correlations, as seen on Fig. 3 and Table 2. The assignments for compound **23** were confirmed by comparison with published NMR data [15,32].

The orientation of the hydroxyl and ethoxyl functionalities at C-9 and C-10 of compound **11** were determined by comparison with the ^{13}C values of the two diastereomers previously reported [33].

2.3. Biological activity

2.3.1. Affinity to cannabinoid receptors

The control used in both binding and functional assays was the non-traditional cannabinoid, CP 55,940 [34]. The binding Ki for CP 55,940 at CB_1 is 0.5–5 nM, and the binding Ki for CP 55,940 at CB_2 is 0.69–2.8 nM. The functional Ki for agonism for this control at the CB_1 receptor is 0.07–4 nM, and 0.2–7.4 nM for CB_2.

Derivatives **13**, **18**, **19**, **21**, **27** and **29** have shown affinity for cannabinoid receptors in the low micromolar and nanomolar

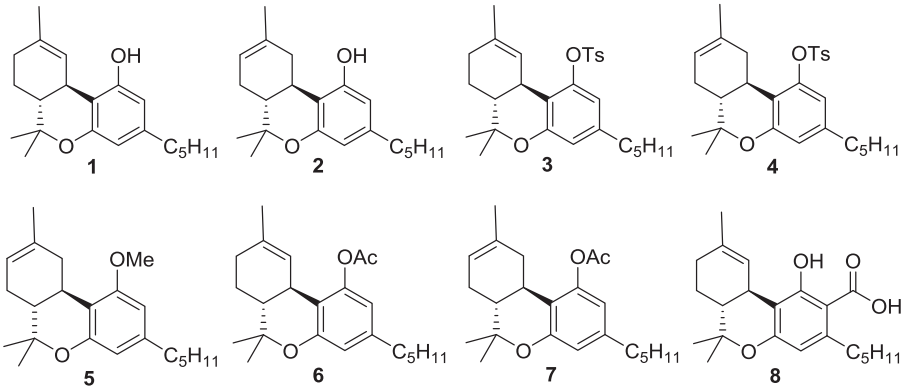

Fig. 1. Structures of Δ^9-THC (**1**), Δ^8-THC (**2**), Δ^9-THC tosylate (**3**), Δ^8-THC tosylate (**4**), Δ^8-THC methoxy (**5**), Δ^9-THC acetate (**6**), Δ^8-THC acetate (**7**), and Δ^9-THCA (**8**).

Table 1
Reaction time, solvent systems and products of photooxygenation of THC derivatives.

Starting material	Solvent system	Reaction time	Product(s)	Scheme
1	CH_2Cl_2/EtOH	11 h	**9**–**12**	1
2	hexanes/CH_2Cl_2 (4:1)	8 h and 30 min	**13**	1
2	CH_2Cl_2/propanol (1:1)	4 h and 30 min	**14**	1
3	CH_2Cl_2	4 h and 15 min	**15, 16, 17,** and **18**	2
3	CH_2Cl_2/EtOH	11 h and 30 min	**17, 18, 19**[a] and **20**	2
4	CH_2Cl_2/EtOH	4 h and 15 min	**21, 22** and **23**[b]	3
5	CH_2Cl_2/EtOH	6 h	**23**–**25**	4
6	hexanes/CH_2Cl_2	4 h	**26**–**30**	5
7	hexanes/CH_2Cl_2	8 h and 15 min followed by reduction with $NaBH_4$	**27**	5
8	CH_2Cl_2/MeOH (1:1)	3 h	**28**	4

[a] Product of reduction of **18**.
[b] product of hydrolysis of **21**.

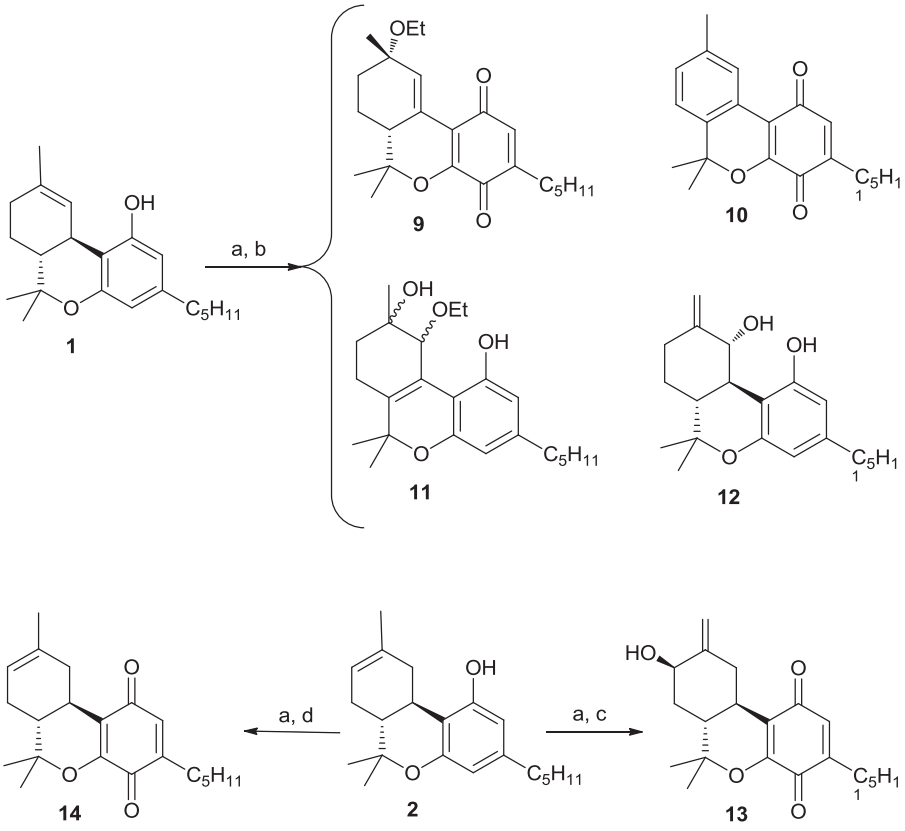

Scheme 1. Synthesis of compounds **9**–**14**.
Reagents and conditions: (a) *meso*-tetraphenylporphine, O_2, light, (b) CH_2Cl_2/anhydrous EtOH (1:2), 11 h; (c) hexanes/CH_2Cl_2 (4:1), 8 h and 30 min; (d) CH_2Cl_2/n-propanol (1:1), 4 h and 30 min.

range.

Emax of compound 21 at 100 μM was 20% stimulation for CB_1 and 90% for CB_2. Compound 29, also at 100 μM, exhibited an Emax of 20% stimulation for CB_1 and 40% for CB_2. Table 3 presents the most representative values of binding affinity to CB_1 and CB_2 and Table 4 presents the most representative results from functional assays.

Compounds **18** (C1 tosylate, C10 hydroperoxide), **19** (C1 tosylate, C10 hydroxyl) and **29** (C9 methoxy, C1 and C10 hydroxyl) showed a relatively high affinity for CB_2 receptors, with IC_{50} of the order of 0.5–0.6 μM whereas their affinity for CB_1 receptors was at and slightly above 1 μM.

Addition of hydroxyl groups to C9 seems to improve affinity for both cannabinoid receptors, but the state of the hydroxyl group at C1 (tosylated or free) seems to make a difference in selectivity. Compound **21**, a C9 hydroperoxide tosylate derivative, displayed good affinity for the CB_1 receptors with IC_{50} lower than 100 nM, and lower affinity for CB_2. Compound **23**, a diol with a hydroxyl group at C9 and free hydroxyl at C1, displayed marked and selective binding affinity for CB_2 receptor with an IC_{50} lower than 20 nM, and lower affinity for CB_1, with an IC_{50} of the order of 1 μM. Compound **27**, a C9-C10 epoxide with the hydroxyl group at C-1 masked by an acetate, had the opposite profile, showing higher affinity for the CB_1 receptors with IC_{50} of the order of 0.5 μM and lower affinity for CB_2 receptors, with IC_{50} of the order of 1 μM.

2.3.2. Functional assays on cannabinoid receptors

Cannabinoid receptor assays led to identification of derivatives **7**

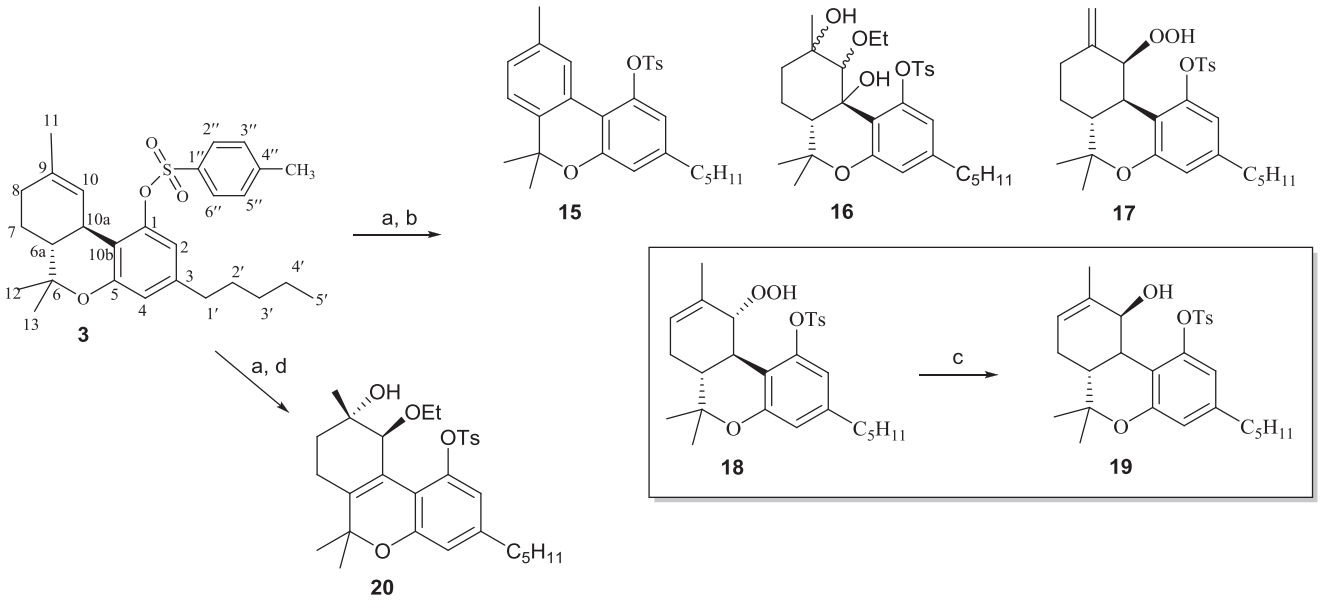

Scheme 2. Synthesis of compounds **15**–**20**.
Reagents and conditions: (a) *meso*-tetraphenylporphine, O_2, light, (b) CH_2Cl_2, 4 h and 15 min; (c) Me_2S/22 h; (d) CH_2Cl_2/abs EtOH (1:1), 11 h and 30min.

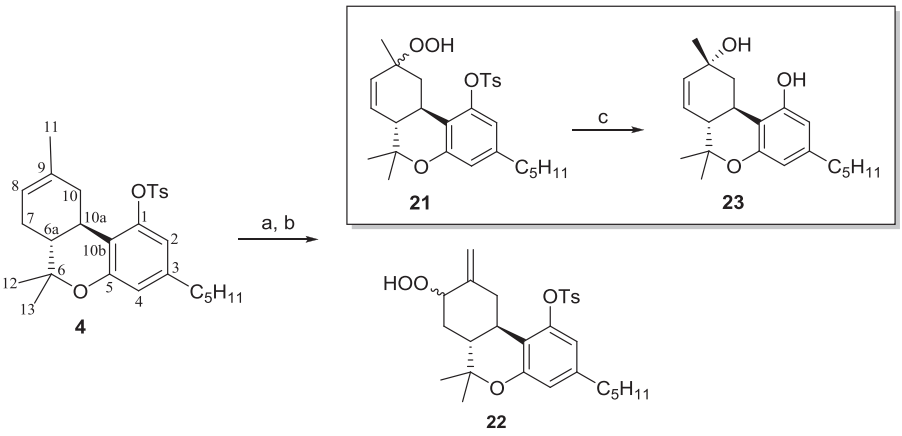

Scheme 3. Synthesis of compounds **21**–**23**.
Reagents and conditions: (a) meso-tetraphenylporphine, O_2, light, (b) CH_2Cl_2/anhydrous EtOH (1:1), 4 h; (c) hydrolysis, KOH/EtOH, 75 min.

and **21** (Table 4) as CB_1 partial agonists, with affinity values in the nanomolar level, and marginal affinity to CB_2.

As previously mentioned, Emax of 21 (100 μM) was 20% for CB1 and 90% for CB2 and 29, also at 100 μM, exhibited an Emax of 20% for CB1 and 40% for CB2.

The aforementioned results revealed that, in contrast to a previous study [35] reporting complete loss of activity when the phenolic hydroxyl group at C-1 of THC is blocked, photooxygenation of acetate and tosylate derivatives yielded oxygenated derivatives with masked hydroxyl groups at C-1 which were found to retain affinity towards the cannabinoid receptors.

1,4-Quinones **24**–**26** did not exhibit any level of affinity towards CB_1 and CB_2, presumably indicating that this functionality may hinder receptor binding due to steric effect.

2.3.3. Anticancer activity

Quinones **9**, **10** [36], **14**, and **25** exhibited anticancer activity against cell lines SK-MEL, KB, BT-549, and SK-OV-3 with IC_{50} values ranging from 4.2 μg/mL (**14**, against BT-549) to 8.65 μg/mL (**25**, against SK-MEL) (Table 5). It is noteworthy to mention that cannabinoid quinone derivatives prepared through KOH/EtOH oxidation [17] have been previously reported to possess antitumor activity, with HU-331 [19] exhibiting its anticancer effect through a novel mechanism of action as topoisomerase II inhibitor.

2.3.4. Antimicrobial activity

Compounds **9**, **10**, **11**, **13**, **14**, **24**–**26**, and **31** exhibited antimicrobial activity against pathogenic bacteria *Staphylococcus aureus*, Methicillin-resistant *Staphylococcus aureus* (MRSA), and pathogenic fungi *Candida glabrata*, *Candida krusei*, and *Cryptococcus neoformans* (Table 6). Compound **14**, a quinone derivative of Δ^8-THC, was found to be the most active anti-cryptococcal agent and also the strongest antibacterial agent against MRSA with IC_{50} of 1.36 μg/mL and MIC 2.50 μg/mL. Compound **25** was the most potent agent against *S. aureus* with IC_{50} 0.91 μg/mL and MIC 2.50 μg/mL. Compounds **9**, **10**, **11**, **13**, **14**, and **31** exhibited considerable activity against

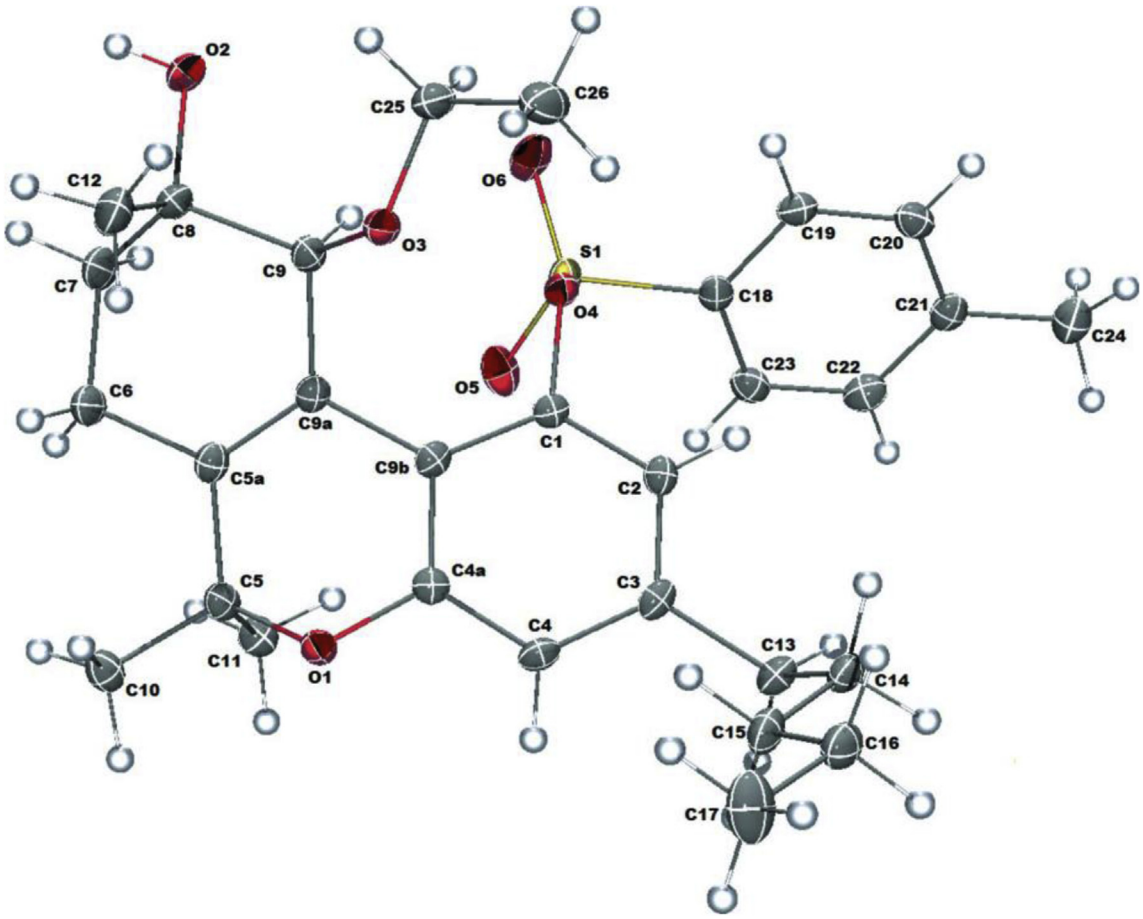

Fig. 2. Plot of the molecular structure of compound **20**, Displacement ellipsoids are drawn at the 50% probability level.

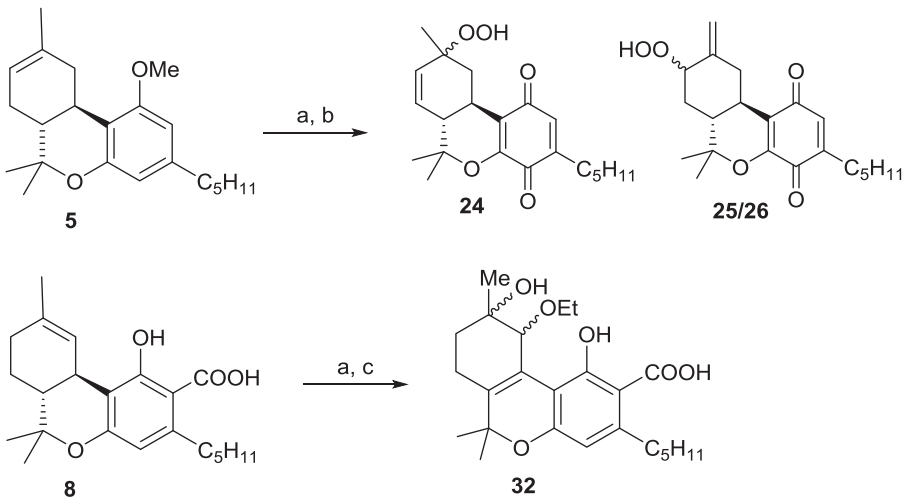

Scheme 4. Synthesis of compounds **32**, **24**–**26**.
Reagents and conditions: (a) *meso*-tetraphenylporphine, O_2, light, (b) CH_2Cl_2/abs EtOH (1:1), 6 h, (c) CH_2Cl_2/MeOH (1:1), 3 h.

C. neoformans, *S. aureus*, and MRSA, without any effect on both *Candida* species tested. Compound **24**, despite not being the most active compound against bacterial strains, exhibited inhibitory activity against all the organisms tested and was the most active against both species of *Candida*.

2.3.5. Antimalarial activity

Among the compounds tested against *Plasmodium falciparum* D6 (chloroquine-sensitive) and W2 (chloroquine-resistant) strains, compound **14** exhibited the highest activity with IC_{50} of 0.16 μg/mL for D6 and IC_{50} of 0.20 μg/mL for W2 (Table 7).

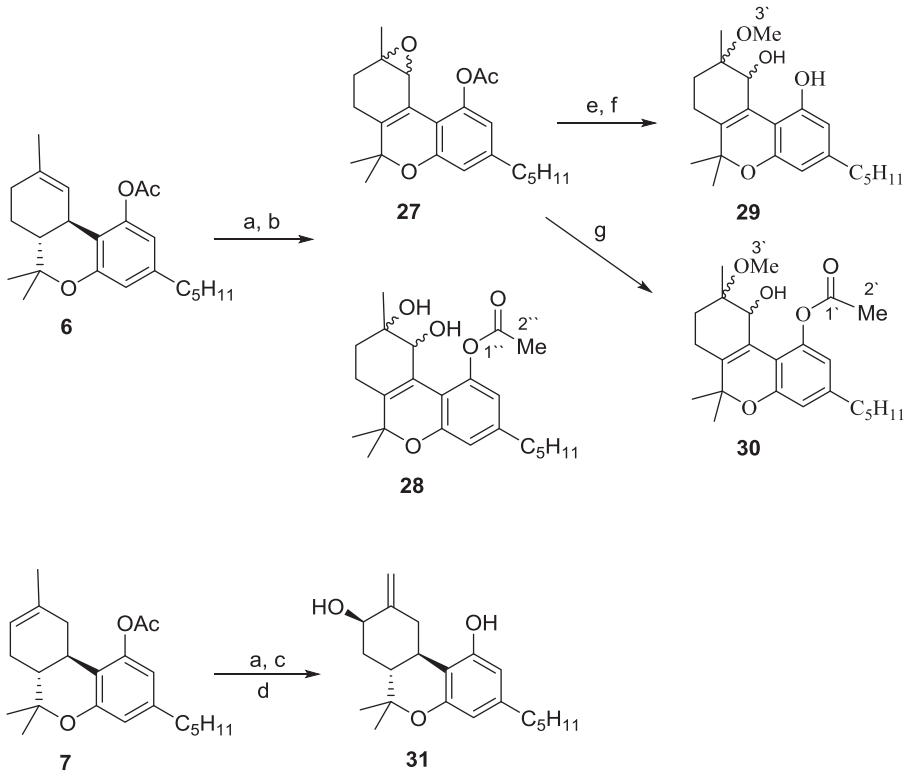

Scheme 5. Synthesis of compounds **27**–**31**.
Reagents and conditions: (a) *meso*-tetraphenylporphine, O_2, light; (b) hexanes/CH_2Cl_2 (1:1), 10 °C, 3 h, 45 min; (c) hexanes/CH_2Cl_2 (1:1), 7.7 °C, 8 h; (d) $NaBH_4$/MeOH, 6 h; (e) $NaBH_4$/MeOH, 2 h, 30 min; (f) $NaHCO_3/H_2O$/MeOH, Adogen 464, (g) Pd/C, H_2, MeOH, 10 h.

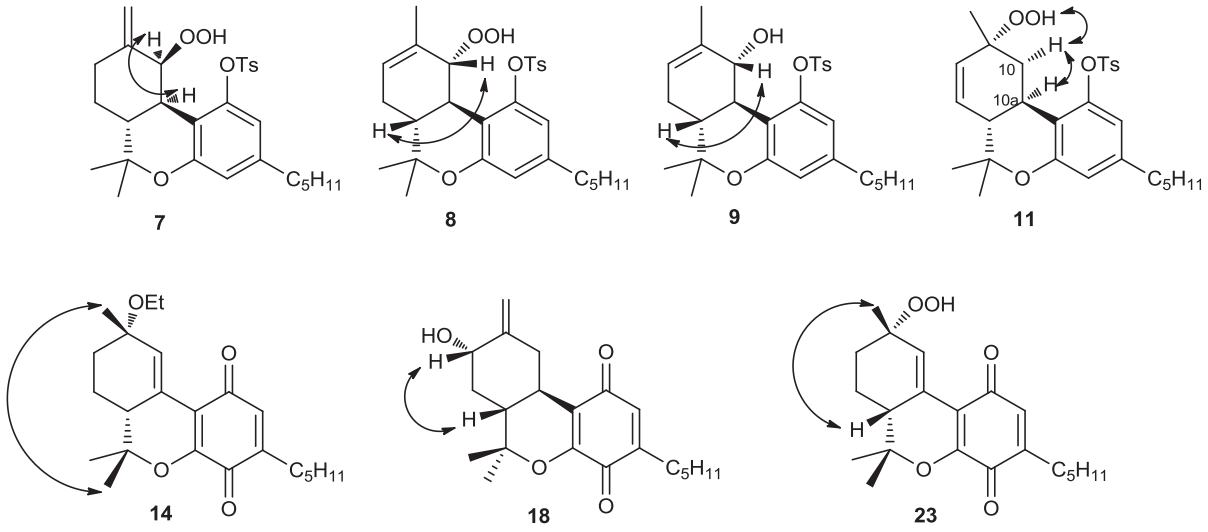

Fig. 3. Relative configuration of compounds **9**, **13, 17**, **18**, **19, 21**, and **24**, based on NOESY correlations.

2.3.6. Antileishmanial activity

Compound **14**, in addition to its antimicrobial and antimalarial effects, also displayed pronounced antileishmanial effect against promastigotes of *Leishmania donovani* with IC_{50} 0.06 μg/mL and $IC_{90\ of}$ 0.13 μg/mL (Table 8). Those inhibitory concentrations are almost three times lower than the standard compound Amphotericin B, placing compound **14** as a good candidate for further studies of its antileishmanial properties.

2.4. Molecular modeling

The two known subtypes of cannabinoid (CB) receptors CB_1 and CB_2 share approximately 44% identity throughout the entire protein sequence and roughly 74% of the seven transmembrane (TM) regions. The structural similarities, principally in the ligand binding cavity, led to non-selective behaviors of many CB modulators. Experimental crystal structure is not available for CB_2 receptor and

Table 2
Stereochemical orientation of derivatives **9**, **13, 17**, **18**, **19, 21**, and **24**., as determined on the basis of NOESY correlations.

Compound	Group analyzed	Orientation	Correlation
9	OEt at C-9	α-oriented	between Me-11 (δ 1.41) at C-9 and Me-13 (δ 1.04 - previously established as β-oriented)
13	OH at C-8	α-oriented	between H-8 (δ 4.14) and the α-oriented Me-12 (δ 1.52).
17	HOO at C-10	β-oriented	between H-10 (δ 4.63) and the α oriented H-10a (δ 2.07)
18	HOO at C-10	α-oriented	between H-10 (δ 4.14) and the β-oriented H-6a (δ 1.79)
19	OH at C-10	α-oriented	between H-10 (δ 4.06) and the β-oriented H-6a (δ 1.74).
21	HOO at C-9	α-oriented	between the proton of HOO (δ 9.28) at C-9 and the α-oriented H-10 (δ 3.52)
	H-10	α-oriented	with H-10a (δ 2.85)
24	HOO at C-9	α-oriented	between Me-11 (δ 1.55 at C-9) and the β-oriented H-6a (δ 2.77)

Table 3
Results of CB_1 and CB_2 binding assays for compounds **7, 14, 18, 19, 21, 22, 23, 27, 29,** and **30**. Error was monitored for each concentration point and displayed on the graphics (supplementary information) with error bars.

Compound	CB_1[a]	CB_2[a]
7	0.088/0.044	0.316/0.158
14	1.84/0.919	4.07/2.034
18	1.024/0.512	0.851/0.426
19	1.28/0.642	1.11 (0.552)
21	0.275/0.137	0.421/0.211
22	5.70/2.85	2.06/1.03
23	0.93/0.47	0.019/0.0095
27	0.573/0.286	0.927/0.464
29	1.077/0.538	0.599/0.300
30	2.80/1.40	1.98/0.99
CP 55,940	-/0.0005–0.005	-/0.00069–0.0028

[a] Values are expressed as IC_{50}/Ki in μM.

Table 4
Results of CB_1 and CB_2 functional assays for compounds **7**, **21**, and **23.** The radioligand used was [35S]-GTP-ϒS, from Perkin Elmer. Error was monitored for each concentration point and displayed on the graphics (supplementary information) with error bars.

Compound	CB_1[a]	CB_2[a]
7	0.087/0.043	0.518/0.259
21	0.097/0.048	1.75/0.876
23	0.387/0.193	11.42/5.70
CP 55,940	-/0.0007–0.004	0.0002–0.0074

[a] Values are expressed as IC_{50}/Ki in μM.

homology models were built to be used in the study.

3D models were validated by inspecting dihedral angles, bond length, planarity and other criteria of structural quality assessment. Molecular docking was performed to investigate the binding pattern of our compounds. The effects of structural modifications of the phenolic hydroxyl group at C1, aliphatic chain at C3, and aliphatic hydroxylation at C9 of classical CB modulators are thoroughly studied showing their importance for CB activity. Several of the active compounds lack some of these structural elements, and therefore we tried to understand how these compounds interact with CB receptors.

Compounds **18**, **19** and **29** showed better fitting in the active site of CB_2 compared to CB_1 as implied by lower docking scores. Compounds **7, 21** and **23** showed docking scores of −7.4, −10 and −9.1 kcal/mol in CB_1, and -7, -5.1 and −7.1 kcal/mol in CB_2.

The interaction models of compound **21** in CB1 (Figs. 4 and 5) demonstrated H-bonds with Ser383 and His178, π-π stacking with Phe170, and hydrophobic contacts with the surrounding amino acids in the binding pocket.

Compound **7** presented π-π stacking with Phe170 and multiple hydrophobic interactions with the amino acid residues of CB_1, while compound **23** displayed strong H-bonding with Ser285, π-π stacking with Phe183 and Phe87, and several hydrophobic contacts with the surrounding amino acids of CB_2 (Figs. 4 and 5).

We explored the stability of the docking poses of **7, 21** and **23** with molecular dynamics (MD) simulations. The protein-ligand interactions were investigated throughout the course of MD simulations. Protein structures were converged after a short MD period as calculated by the root mean square deviation (RMSD) of backbone, side chains and heavy atoms (Fig. 5), indicating that the production stage was reached. The RMSD values, over 40 ns, showed a fluctuation within 1–2 Å after the equilibration period confirming system stability.

Compound **21** demonstrated hydrophobic contacts with the surrounding amino acid residues in the binding pocket of CB_1. His178 forms a well-preserved H-bond with the sulfonyl oxygen of the tosylate group (~56% of the simulation time) and the peroxy group shows intramolecular hydrogen bond with the same sulfonyl oxygen (~50%). His178, Phe170 and Phe288 make π-π stacking

Table 5
Anticancer activity of compounds **9, 10, 14, 25 and 26**, expressed as IC_{50} of growth inhibition (μg/mL).

Compound	Cancer Cells				Noncancer Cells	
	SK-MEL	KB	BT-549	SK-OV-3	VERO	$LLC\text{-}PK_1$
9	6.2 ± 0.28	NA	5.3 ± 0.70	NA	5.95 ± 0.78	5.4 ± 0.42
10	7.6 ± 0.85	NA	6.05 ± 0.49	NA	NT	5.65 ± 0.07
14	NT	5.25 + 0.35	4.2 + 0.28	4.35 + 0.21	4.1 + 0.42	2.25 + 0.07
25	8.65 ± 0.49	NA	NA	NA	NT	9.9 ± 0.14
26	NA	NA	NA	NA	NT	9.95 ± 0.07

SK-MEL: Human melanoma.
KB: Human epidermal carcinoma, oral.
BT-549: Ductal carcinoma, breast.
SK-OV -3: Human ovary carcinoma.
VERO: Monkey kidney fibroblasts.
LLC-PK1: Pig kidney epithelial cells.
Values are average of two determinations ± std dev.
NA = no activity up to 10 μg/mL.
NT = not tested.

Table 6
Antimicrobial activity of compounds **9**, **10**, **11**, **13**, **14**, **24**, **25**, **26** and **31** expressed as IC_{50}/MIC (μg/mL).

Compound	*Candida glabrata*	*Candida krusei*	*Cryptococcus neoformans*	*Staphylococcus aureus*	MRSA
9	–/–	–/–	0.88/-	2.04/-	2.04/-
10	–/–	–/–	4.44/20.0	>20/-	–/–
11	–/–	–/–	4.57/-	4.86/-	17.07/-
13	–/–	–/–	1.84/5.00	2.03/2.50	5.53/10.0
14	–/–	–/–	0.70/2.50	1.35/2.50	1.36/2.50
24	6.54/10.0	5.77/10.0	0.93/2.50	1.30/2.50	2.63/5.0
25	–/–	17.0/-	1.40/2.50	0.91/2.50	5.78/10.0
26	–/–	20.0/-	2.05/5.0	2.41/5.0	15.3/-
31	–/–	–/–	8.34/-	10.71/-	–/–
Amphotericin B	–/–	–/–	1.36/2.50	–/–	–/–
Ciprofloxacin	–/–	–/–	–/–	0.11/0.25	0.12/0.25

Table 7
Antimalarial activity of compounds **1**–**10**, **17**, **19**–**21**, represented as IC_{50} (μg/mL).

Compound	9	11	14	20	25	28	30	31	Chloroquine	Artemisinin
P. falciparam (D6 strain)	4.76	3.6	0.160	2.2	1.0	4.50	3.3	2.4	0.016	0.013
P. falciparam (W2 strain)	4.50	3.7	0.20	1.8	0.90	3.20	3.0	1.7	0.140	0.014

D6: chloroquine-sensitive strain.
W2: chloroquine-resistant strain.

Table 8
Antileishmanial activity of compounds **9**, **11**, **13**, **14**, **17**, **20**, **24**, **25**, **26** and **29** presented as IC_{50} and IC_{90} (μg/mL).

Compound	9	11	13	14	17	20	24	25	26	29	Pentamidine	Amphotericin B
IC_{50}	0.5	3.0	0.6	0.06	3.1	4.5	0.7	2.1	3.1	35	1.0	0.16
IC_{90}	3.0	6.0	1.3	0.13	6.5	22	1.2	11	8	>40	2.0	0.33

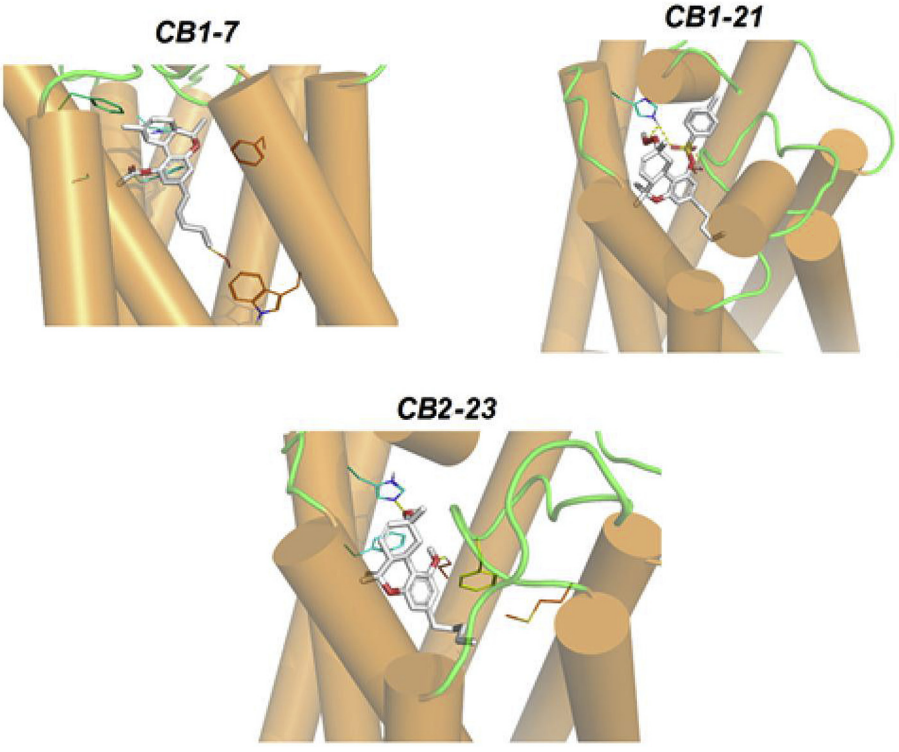

Fig. 4. 3D interaction models of compounds **7** (CB1-7) and **21** (CB1-21) with CB_1, and compound **23** (CB2-23) with CB_2. The protein is displayed as orange α-helices and green loops. The ligands are shown as white sticks, and surrounding amino acids as lines. (For interpretation of the references to colour in this figure legend, the reader is referred to the web version of this article.)

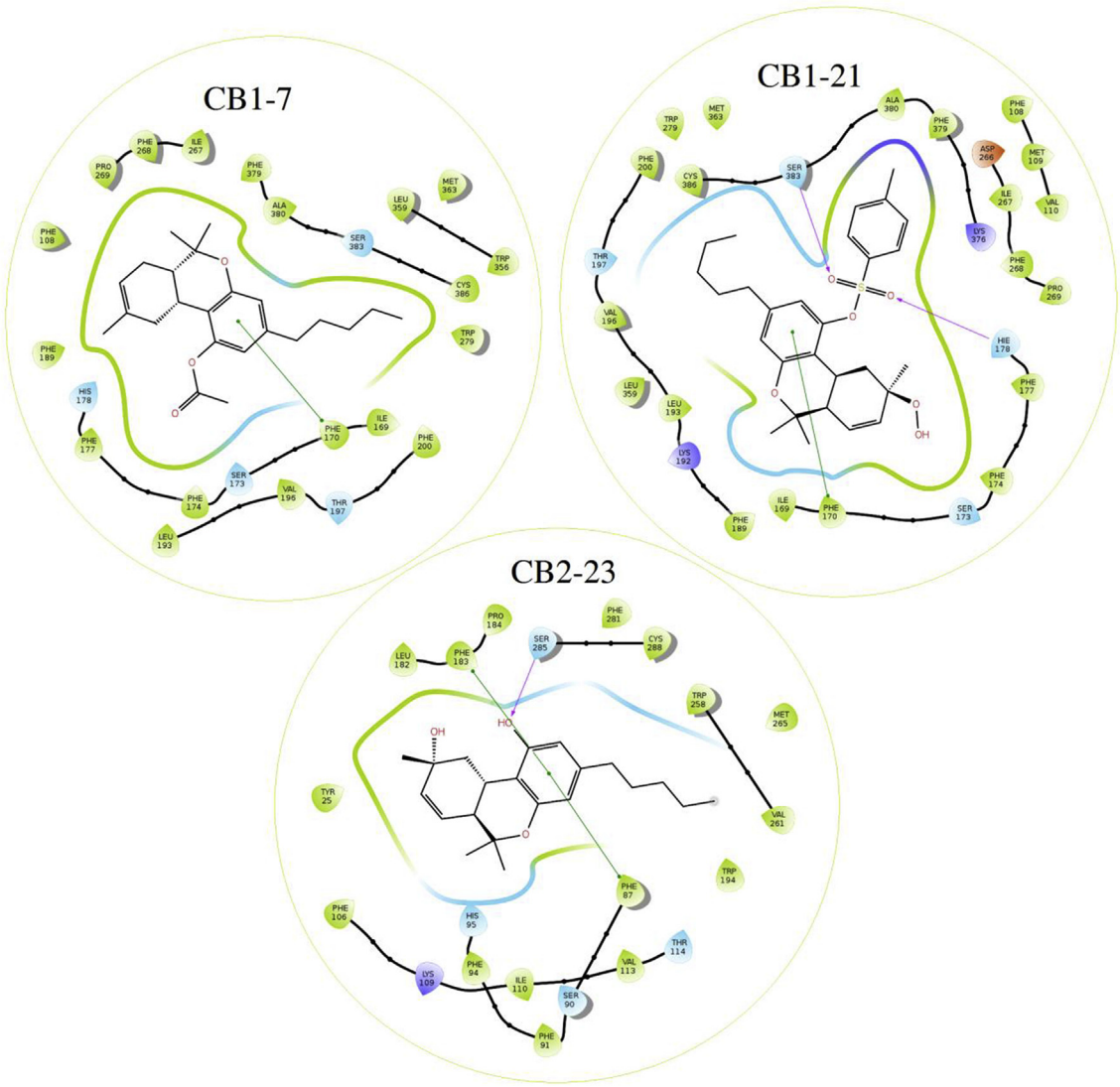

Fig. 5. 2D interaction models of compounds **7** (CB1-7), **21** (CB1-21) and **23** (CB2-23). H-bonds are shown as purple lines. π-π stacking is shown as green dashed lines with green spheres at the ends. Hydrophobic interactions are displayed as solid green lines. (For interpretation of the references to colour in this figure legend, the reader is referred to the web version of this article.)

(~23%, 44% and 18%, respectively) with the aromatic rings. Blocking the phenolic hydroxyl group at C1 with toyslate group did not abolish the CB activity of compound **21**. The toyslate group offered favorable molecular region for CB interactions. The sulfonyl group acted in part as the free phenolic hydroxyl group and formed strong H-bond with His178 and Ser383, and the tosylate aromatic group formed π-π stacking with His178.

Hydrophobic contacts are very important for compound **7** with CB_1. Phe108, Phe170 and Leu193 display strong hydrophobic interactions with ligand atoms. Compound **23** strongly binds to CB_2 through H-bonds with His95 (~94%) and Ser285 (~99%), and hydrophobic contacts with Phe87 (~19%) and Phe183 (~73%).

3. Conclusion

Photooxygenation of Δ^9-THC, Δ^8-THC, Δ^9- THCA and derivatives resulted in the formation of 24 oxygenated products with diversified functionalities, some of them previously reported as minor constituents in *Cannabis* or its metabolites [37]. Change of reaction time and solvent systems led to the formation of different products. Compounds **7** and **21** were recognized as selective CB_1 partial agonists, demonstrating that blockade of the C-1 hydroxyl function of the cannabinoid structure does not necessarily abolish affinity towards cannabinoid receptors.

Cannabinoid receptor binding and functional assays also demonstrated that the introduction of the 1,4-quinone moiety (compounds **9**, **10**, **14** and **24**–**26**) led to loss of affinity towards cannabinoid receptors CB_1 and CB_2. Those same quinone derivatives, however, were the only derivatives exhibiting anticancer and marked antimicrobial activity. Quinone **14** was the most potent anti-cryptococcal and anti-MRSA agent, **25** was the best agent against *S. aureus* and quinones **24**–**26** showed anticandidal activity. **9**, **10**, **11**, **13**, **14** and **31** showed antimicrobial activity against *C. neoformans*, *S. aureus*, and MRSA, without any effect on the *Candida* species tested.

Compounds **21**, **23** and the quinone derivatives **9**, **10**, **14** and **24**–**26** bear promising bioactivities warranting further pursuit focusing on improving yields and increasing selectivity of the reactions.

4. Experimental protocols

4.1. Chemistry

Starting materials Δ^9-THC, Δ^8-THC, and Δ^9-THCA were isolated from *Cannabis sativa* [38] grown in the Medicinal Plant Garden at the University of Mississippi, Mississippi, USA and authenticated by Dr. Suman Chandra [39]. 1D and 2D NMR spectra were recorded in $CDCl_3$ as a solvent on a Bruker Avance DPX-400 spectrometer and on a Varian AS 400 spectrometer. HRESIMS was obtained using a Bruker Bioapex FTMS in ESI mode. LRESIMS was obtained using a 3200 Q Trap LC/MS/MS (Applied Biosystems MDS Sciex, Foster City, CA). TLC was carried out on aluminum-backed plates precoated with silica gel F_{254} (20 × 20 cm, 200 μm, 60 Å, Merck). Visualization was accomplished by spraying with fast blue or p-anisaldehyde [0.5 mL in glacial acetic acid (50 mL) and H_2SO_4 (97%, 1 mL)] spray reagent followed by heating. Flash silica gel (40–63 μm, 60 Å, Silicycle) and SiliaBond C18 silica gel (40–63 μm, 60 Å, 17% carbon loading, Silicycle) were used for column chromatography.

4.2. General experimental conditions

Δ^9-THC, Δ^8-THC were converted to the tosylate [25], acetate [40,41] esters or methyl ether [42] prior to photooxygenation, In addition, free cannabinoids and Δ^9-THCA were also subjected to photooxygenation. For the photooxygenation reactions, *meso*-tetraphenylporphine (1.0 mg) was added to the appropriate THC derivative dissolved in a solvent or mixture of solvents. The reaction mixture was irradiated with 500 W incandescent light for the appropriate amount of time, with oxygen being gently bubbled into the solution and the temperature of the reaction bath maintained at 10–13 °C. At the end of the reaction, the solvent was removed and the mixture purified by column chromatography, unless otherwise specified.

Progress of the reactions was monitored by TLC. Free cannabinoids on the TLC plates were visualized with fast blue, while tosylate derivatives were detected with *p*-anisaldehyde/H_2SO_4. The identity of these compounds was deduced from spectral analysis including specific rotation, NMR (1D and 2D), and HRESMS.

Compounds **10**, **12**, **14**, **15**, **23** and **31** along with their spectral data have been previously published [15,24–26].

4.2.1. (6aR,10aS)-10-ethoxy-9,10a-dihydroxy-6,6,9-trimethyl-3-pentyl-6a,7,8,9,10,10a-hexahydro-6H-benzo[c]chromen-1-yl 4-methylbenzenesulfonate ***(16)***

Following the general experimental conditions, 2 (800 mg, 1.17 mmol) dissolved in dichloromethane (50 mL), was irradiated for 4 h and 45 min to afford compound 16 (70 mg, 7.8%) as a resinous matter; R_f = 0.72 (Hexanes- EtOAc, 7:3); $[\alpha]^{26}_D$ = 15.5 (*c* 0.11, MeOH); ^{1}H NMR (400 MHz, $CHCl_3$, TMS) δ: 0.88 (distorted t, 3H, Me-5′), 1.34 (s, 3H, Me-12), 1.26 (brs, Me-15), 1.32 (s, 3H, Me-11), 1.37 (s, 3H, Me-13), 2.43 (s, 3H, Me-4″), 3.57 (m, 2H, H-14a and H-14b), 3.69 (brs, 1H, H-10), 6.46 (brs, 1H, H-2), 6.54 (brs, 1H, H-4), 7.31 (brs, 2H, H-3″, H-5″), 7.90 (brs, 2H, H-2″, H-6″); ^{13}C NMR (Table 1); HRESIMS *m/z* 546.2785 $[M]^-$ (calcd for $C_{30}H_{42}O_7S$, 546.2651).

4.2.2. (6aR,10S,10aR)-10-hydroperoxy-6,6-dimethyl-9-methylene-3-pentyl-6a,7,8,9,10,10a-hexahydro-6H-benzo[c]chromen-1-yl 4-methylbenzenesulfonate ***(17)***

Following the general experimental conditions, **2** (800 mg, 1.17 mmol) dissolved in dichloromethane (50 mL), was irradiated for 4 h and 45 min to afford compound **17** (118 mg, 14.1%) as a resinous matter; R_f = 0.36 (Hexanes- EtOAc, 80:20); $[\alpha]^{26}_D$ = −22.0 (*c* 0.10, MeOH); ^{1}H NMR (400 MHz, $CHCl_3$, TMS) δ: 0.87 (t, *J* = 7 Hz, 3H, Me-5′), 0.81 (s, 3H, Me-13), 1.31 (s, 3H, Me-12), 1.46 (1H, m, H-6a), 2.07 (1H, dd, J = 4 and 12.8 Hz, H-10a), 2.41 (s, 3H, Me-4″), 5.00 (s, 1H, H-11a), 5.10 (s, 1H, H-11b), 4.63 (d, *J* = 2.4 Hz, 1H, H-10), 6.32 (d, *J* = 1.6 Hz, 1H, H-2), 6.49 (d, 1.2 Hz, 1H, H-4), 7.257 (d, *J* = 8.4 Hz, 2H, H-3″, H-5″), 7.69 (d, *J* = 8.4 Hz, 2H, H-2″, H-6″), 8.12 (s, 1H, HOO-10); ^{13}C NMR (Table 1); HRESIMS *m/z* 501.2311 $[M+H]^+$ (calcd for $C_{28}H_{37}O_6S$, 501.2278).

4.2.3. (6aR,10R,10aR)-10-hydroperoxy-6,6,9-trimethyl-3-pentyl-6a,7,10,10a-tetrahydro-6H-benzo[c]chromen-1-yl 4-methylbenzenesulfonate ***(18)***

Following the general experimental conditions, **2** (800 mg, 1.17 mmol) dissolved in dichloromethane (50 mL), was irradiated for 4 h and 45 min to afford compound **18** (87 mg, 10.4%) as a resinous matter; R_f = 0.50 (Hexanes- EtOAc, 80:20); $[\alpha]^{26}_D$ −39.2 (*c* 0.125, MeOH); ^{1}H NMR (400 MHz, $CHCl_3$, TMS) δ: 0.74 (s, 3H, Me-13), 0.87 (t, *J* = 7.2 Hz, 3H, Me-5′), 1.31 (s, 3H, Me-12), 1.79 (br dd, *J* = 8.6 Hz, 1H, H-6a), 1.89 (s, 3H, Me-11), 2.40 (s, 3H, Me-4″), 3.05 (t, *J* = 8.4 Hz, 1H, H-10a), 4.14 (d, *J* = 8.8 Hz, 1H, H-10), 5.75 (d, *J* = 6.0, 1H, H-8), 6.29 (d, *J* = 1.60 Hz, 1H, H-2), 6.52 (s, 1H, H-4), 7.26 (d, *J* = 8.0 Hz, 2H, H-3″, H-5″), 7.66 (d, *J* = 8.4 Hz, 2H, H-2″, H-6″), 9.20 (s, 1H, HOO-10); ^{13}C NMR (Table 1); HRESIMS *m/z* 483.2227 $[M-OH]^+$ (calcd for $C_{28}H_{35}O_5S$, 483.2205).

4.2.4. (6aR,10S)-10-hydroxy-6,6,9-trimethyl-3-pentyl-6a,7,10,10a-tetrahydro-6H-benzo[c]chromen-1-yl 4-methylbenzenesulfonate ***(19)***

13 mg, 0.026 mmol, of **18** was added to 1 mL of Me_2S and the mixture was stirred for 22 h at room temperature. The reaction mixture was concentrated under *vacuum* to yield 11 mg (87.3%) of compound **19** as a viscous brownish yellow oil; R_f = 0.40 (Hexanes-EtOAc, 80:20); ^{1}H NMR (400 MHz, $CHCl_3$, TMS) δ: 0.80 (s, 3H, Me-13), 0.92 (t, *J* = 8.6 Hz, 3H, Me-5′), 1.34 (s, 3H, Me-12), 1.81 (s, 3H, Me-11), 2.43 (s, 3H, Me-4″), 2.62 (overlapped with DMSO signal (1H, H-10a), 4.06 (d, *J* = 6.3 Hz, 1H, H-10), 5.60 (d, *J* = 5.5, 1H, H-8), 6.48 (br d 1H, H-2), 6.50 (br d, 1H, H-4), 7.28 (d, *J* = 8.3 Hz, 2H, H-3″, H-5″), 7.71 (d, *J* = 8.3 Hz, 2H, H-2″, H-6″),; ^{13}C NMR (Table 1); HRESIMS *m/z* 483.2227 $[M-OH]^+$ (calcd for $C_{28}H_{35}O_5S$, 483.2205).

4.2.5. (9S,10S)-10-ethoxy-9-hydroxy-6,6,9-trimethyl-3-pentyl-7,8,9,10-tetrahydro-6H-benzo[c]chromen-1-yl 4-methylbenzenesulfonate ***(20)***

Following the general experimental conditions, **3** (1.5 g, 2.19 mmol) dissolved in a mixture of dichloromethane (25 mL) and anhydrous ethanol (25 mL) was irradiated for 11 ½ h to afford compound **20** (291 mg, 17.2%) as an amorphous solid; R_f = 0.35 (Hexanes- EtOAc, 70:30); $[\alpha]^{26}_D$ = −24.0 (*c* 0.10, MeOH); ^{1}H NMR (400 MHz, $CHCl_3$, TMS) δ: 0.84 (t, *J* = 6.4 Hz, 3H, Me-5′), 0.88 (s, 3H, Me-12), 1.03 (t, *J* = 6.8 Hz, Me-15), 1.23 (s, 3H, Me-11), 1.37 (s, 3H, Me-13), 2.35 (s, 3H, Me-4″), 3.66 (m, 1H, H-14a), 3.90 (m, 1H, H-14b), 4.5 (s, 1H, H-10), 6.37 (d, *J* = 1.2, Hz, 1H, H-2), 6.53 (d, *J* = 1.6 Hz, 1H, H-4), 7.22 (d, *J* = 8.0 Hz, 2H, H-3″, H-5″), 7.64 (d, *J* = 8.0 Hz, 2H, H-2″, H-6″); ^{13}C NMR (Table 1); HRESIMS *m/z* 527.2484 $[M-H]^-$ (calcd for $C_{30}H_{39}O_6S$, 527.2481).

4.2.6. (6aR,10aR)-9-hydroperoxy-6,6,9-trimethyl-3-pentyl-6a,9,10,10a-tetrahydro-6H-benzo[c]chromen-1-yl 4-methylbenzenesulfonate ***(21)***

Following the general experimental conditions, **4** (1.0 g, 2.14 mmol) dissolved in a mixture of dichloromethane (30 mL) and anhydrous ethanol (15 mL) was irradiated for 4 h and 15 min to afford compound **21** (117 mg, 13.7%) as a resinous matter; R_f = 0.44 (Hexanes- EtOAc, 80:20); $[\alpha]^{26}_D$ - 33 (*c* 0.10, MeOH); ^{1}H NMR (400 MHz, $CHCl_3$, TMS) δ: 0.87 (t, *J* = 6.0 Hz, 3H, Me-5′), 0.87 (s, 3H, Me-13), 1.43 (s, 3H, Me-11), 1.43 (s, 3H, Me-12), 2.09 (brd,

J = 10.8 Hz, 1H, H-6a), 2.40 (s, 3H, Me-4″), 2.85 (brt, J = 10.0 Hz, H-10a), 5.62 (brd, J = 9.6 Hz, 1H, H-7), 5.90 (brd, J = 10 Hz, 1H, H-8), 6.11 (brs, 1H, H-2), 6.53 (brs, 1H, H-4), 7.28 (d, J = 8.4 Hz, 2H, H-3″, H-5"), 7.71 ((d, J = 8.8 Hz, 2H, H-2", H-6"), 9.28 (s, 1H, HOO-9); ^{13}C NMR (Table 1); HRESIMS *m/z* 523.2118 $[M+Na]^+$ (calcd for $C_{28}H_{36}O_6SNa$, 523.2233).

4.2.7. (6aR,10aR)-8-hydroperoxy-6,6-dimethyl-9-methylene-3-pentyl-6a,7,8,9,10,10a-hexahydro-6H-benzo[c]chromen-1-yl 4-methylbenzenesulfonate (22)

Following the general experimental conditions **4** (1.0 g, 2.14 mmol), dissolved in a mixture of dichloromethane (30 mL) and anhydrous ethanol (15 mL), was irradiated for 4 h and 15 min to afford compound **22** (249 mg, 29.1%) as a resinous matter; R_f = 0.25 (Hexanes- EtOAc, 80:20); $[\alpha]^{26}_D$ = - 61.9 (*c* 0.10, MeOH); ^{1}H NMR (400 MHz, $CHCl_3$, TMS) δ: 0.852 (t, J = 6.8 Hz, 3H, Me-5′), 0.78 (s, 3H, Me-13), 1.43 (s, 3H, Me-11), 1.31 (s, 3H, Me-12), 1.47 (m, 1H, H-6a), 2.37 (s, 3H, Me-4″), 3.48 (dd, J = 13.4, 3.6 Hz, H-10a), 3.48 (dd, J = 3.6, 13.4 Hz, 1H, H-10a), 4.40 (m, 1H, H-8), 4.94 (s, 1H, H-11′), 5.01 (s, 1H, H-11), 6.44 (d, J = 6.4 Hz, 1H, H-2), 6.50 (brs, 1H, H-4), 7.25 (d, J = 7.6 Hz, 2H, H-3″, H-5"), 7.66 (d, J = 8.0 Hz, 2H, H-2", H-6"), 9.28 (s, 1H, HOO at C9); ^{13}C NMR (Table 1); HRESIMS *m/z* 501.2302 $[M+H]^+$ (calcd for $C_{28}H_{37}O_6S$, 501.2266).

4.2.8. (6aR,9R,10aR)-6,6,9-trimethyl-3-pentyl-6a,9,10,10a-tetrahydro-6H-benzo[c]chromene-1,9-diol (23)

Compound **21** (47 mg, 0.094 mmol), dissolved in 5 mL of 10% KOH in ethanol, was refluxed for 75 min, affording compound **23** (25 mg, 80.6%) as a resinous matter; R_f = 0.17 (Hexanes- EtOAc, 75:25); $[\alpha]^{26}_D$ −17 (*c* 0.10, MeOH); ^{1}H NMR (400 MHz, $CHCl_3$, TMS) δ: 0.88 (t, J = 7.2 Hz, 3H, Me-5′), 0.95 (s, 3H, Me-13), 1.38 (s, 3H, Me-11), 1.44 (s, 3H, Me-12), 2.14 (d, J = 10.8 Hz, 1H, H-6a), 3.50 (d, J = 13.6 Hz, 1H, H-10a), 5.78 (m, 2H, H-7, H-8), 6.20 (brs, 1H, H-2), 6.21 (brs, 1H, H-4); ^{13}C NMR (Table 2).

4.2.9. (6aR,9S)-9-ethoxy-6,6,9-trimethyl-3-pentyl-6a,7,8,9-tetrahydro-1H-benzo[c]chromene-1,4(6H)-dione (9)

Following the general experimental conditions, **1** (800 mg, 2.55 mmol) dissolved in a mixture of dichloromethane (25 mL) and anhydrous ethanol (50 mL) was irradiated for 11 h to yield compound **9** (102 mg, 11%) as a resinous matter; R_f = 0.46 (Hexanes-EtOAc, 85:15); $[\alpha]^{26}_D$ −60.9 (*c* 0.16, MeOH); ^{1}H NMR (400 MHz, $CHCl_3$, TMS) δ: 0.87(distorted t, 3H, Me-5′), 1.04 (s, 3H, Me-13), 1.097 (t, J = 7.2 Hz, 3H, Me-2″), 1.22 (s, 3H, Me-12), 1.41 (s, 3H, Me-11), 2.27 (1H, H-6a), 3.38 (q, J = 6.8 Hz, 2H, CH_2-1″), 6.25 (s, 1H, H-2), 7.10 (s, 1H, H-10); ^{13}C NMR (Table 2); HRESIMS *m/z* 371.2368 $[M+H]^+$ (calcd for $C_{23}H_{33}O_4$, 371.2222).

4.2.10. 10-ethoxy-6,6,9-trimethyl-3-pentyl-7,8,9,10-tetrahydro-6H-benzo[c]chromene-1,9-diol (11)

Following the general experimental conditions, **1** (800 mg, 2.55 mmol) dissolved in a mixture of dichloromethane (25 mL) and anhydrous ethanol (50 mL) was irradiated for 11 h to yield compound **11** (48 mg, 5.0%) as a resinous matter; R_f = 0.30 (Hexanes-EtOAc-MeOH, 10:10:0.2); $[\alpha]^{26}_D$ = −20.0 (*c* 0.11, MeOH); ^{1}H NMR (400 MHz, $CHCl_3$, TMS) δ: 0.84 (t, J = 6.8 Hz, 3H, Me-5′), 1.42 (s, 3H, Me-13), 1.15 (t, J = 7.2 Hz, 3H, Me-15), 1.34 (s, 3H, Me-11), 1.24 (s, 3H, Me-12), 3.50 (m, 2H, CH_2-14), 4.2 (s, 1H, H-10), 6.21 (s, 1H, H-2), 6.29 (s, 1H, H-4); ^{13}C NMR (Table 2); HRESIMS *m/z* 373.2393 $[M-H]^-$ (calcd for $C_{23}H_{33}O_4$, 373.2379).

4.2.11. (6aR,8R,10aR)-8-hydroxy-6,6-dimethyl-9-methylene-3-pentyl-6a,7,8,9,10,10a-hexahydro-1H-benzo[c]chromene-1,4(6H)-dione (13)

Following the general experimental conditions, **2** (260 mg, 0.83 mmol) dissolved in a mixture of 40 mL of hexanes and 10 mL of dichloromethane was irradiated for 8 h affording compound **13** (15.7 mg, 5.5%). ^{1}H NMR (400 MHz, $CHCl_3$, TMS) δ: 0.88(t, J = 6.2 Hz, 3H, Me-5′), 1.12 (s, 3H, Me-13), 1.52 (s, 3H, Me-12), 1.72 (m, 1H, H-6a), 2.28 (m, H, H-10a), 4.14 (m, 1H, H-8), 5.01 (s, 2H, CH_2-11), 6.36 (s, 1H, H-2); ^{13}C NMR (Table 2); HRESIMS *m/z* 359.1994 $[M-H]^-$ (calcd for $C_{21}H_{28}O_4$, 359.1858).

4.2.12. 10-ethoxy-1,9-dihydroxy-6,6,9-trimethyl-3-pentyl-7,8,9,10-tetrahydro-6H-benzo[c]chromene-2-carboxylic acid (32)

Following the general experimental conditions, **8** (360 mg, 1.0 mmol) dissolved in a mixture of 40 mL of equal parts of MeOH and CH_2Cl_2 was irradiated for 3 1/2 h, resulting in the formation of **32** (94 mg, 22.4%) as a resinous matter; R_f = 0.15 (Hexanes- EtOAc, 70:30); $[\alpha]^{26}_D$ = −43.8 (*c* 0.105, MeOH); ^{1}H NMR (400 MHz, $CHCl_3$, TMS) δ: 0.87(brt, 3H, Me-5′), 1.05 (t, J = 7.0 Hz, 3H, Me-2″), 1.22 (s, 3H, Me-12), 1.35 (s, 3H, Me-11), 1.45 (s, 3H, Me-13), 3.68 (t, J = 7.4 Hz, 1H, H-1″a), 3.80 (t, J = 7.4 Hz, 1H, H-1″b), 5.0 (s, 1H, H-10), 6.29 (s, 1H, H-4), 12.6 (brs, 1H, OH-3″); ^{13}C NMR (Table 2); HRESIMS *m/z* 417.2219 $[M-H]^-$ (calcd for $C_{24}H_{33}O_6$, 417.2277).

4.2.13. (6aR,10aR)-9-hydroperoxy-6,6,9-trimethyl-3-pentyl-6,6a,10,10a-tetrahydro-1H-benzo[c]chromene-1,4(9H)-dione (24)

Following the general experimental conditions, **2** (260 mg, 0.83 mmol) dissolved in a mixture of 40 mL of hexanes and 10 mL of dichloromethane was irradiated for 8 h affording compound **24** (34 mg, 11.4%). Under the same conditions, compound **5** (methylated Δ^8-THC [42] - 800 mg, 2.44 mmol) was dissolved in a mixture of 30 mL of dichloromethane and 20 mL of absolute ethanol and irradiated for 6 h, also forming product **24** (12.5 mg, 14.1%) as a resinous matter; R_f = 0.48 (Hexanes- DCM-MeOH, 9:9:0.8); $[\alpha]^{26}_D$ = −2.3 (*c* 0.110, MeOH); ^{1}H NMR (400 MHz, $CHCl_3$, TMS) δ: 0.86(t, J = 6.2 Hz, 3H, Me-5′), 1.10 (s, 3H, Me-13), 1.34 (s, 3H, Me-12), 1.55 (s, 3H, Me-11), 2.03 (d, J = 10 Hz, 1H, H-6a), 2.74 (m, 1H, H-10a), 5.68 (d, J = 10 Hz, H-7), 5.82 (d, J = 10, 1H, H-8), 6.37 (s, 1H, H-2); ^{13}C NMR (Table 2); HRESIMS *m/z* 383.1779 $[M+Na]^+$ (calcd for $C_{21}H_{28}O_5Na$, 383.1834).

4.2.14. (6aR,10aR)-8-hydroperoxy-6,6-dimethyl-9-methylene-3-pentyl-6a,7,8,9,10,10a-hexahydro-1H-benzo[c]chromene-1,4(6H)-dione (25)

Following the general experimental conditions, **5** (800 mg, 2.44 mmol) was dissolved in a mixture of 30 mL of dichloromethane and 20 mL of absolute ethanol and irradiated for 6 h, forming product **25** (11 mg, 13.6%) as a resinous matter; R_f = 0.42 (Hexanes- DCM-MeOH, 9:9:0.8); $[\alpha]^{26}_D$ = −15.4 (*c* 0.13, MeOH); OR = - 0.020, 2.6 mg/2 mL MeOH; ^{1}H NMR (400 MHz, $CHCl_3$, TMS) δ: 0.88(t, J = 6.0 Hz, 3H, Me-5′), 1.08 (s, 3H, Me-13), 1.47 (s, 3H, Me-12), 1.83 (m, 1H, H-6a), 2.35 (m, 1H, H-10a), 4.54 (brt, 1H, H-8), 5.12 (s, 3H, Me-11b), 5.22 (s, 3H, Me-11a), 5.68 (d, J = 10 Hz, H-7), 5.82 (d, J = 10, 1H, H-8), 6.36 (s, 1H, H-2); ^{13}C NMR (Table 2); HRESIMS *m/z* 327.2012 $[M-HOO]^+$ (calcd for $C_{21}H_{27}O_3$, 327.1960).

4.2.15. (6aR,10aR)-8-hydroperoxy-6,6-dimethyl-9-methylene-3-pentyl-6a,7,8,9,10,10a-hexahydro-1H-benzo[c]chromene-1,4(6H)-dione (26)

Following the general experimental conditions, **5** (800 mg, 2.44 mmol) was dissolved in a mixture of 30 mL of dichloromethane and 20 mL of absolute ethanol and irradiated for 6 h, forming product **26** (10 mg, 12.4%) as a resinous matter; R_f = 0.36 (Hexanes- DCM-MeOH, 9:9:0.8); $[\alpha]^{26}_D$ = −24.0 (*c* 0.10, MeOH); OR = - 0.024, 2.0 mg/2 mL MeOH; ^{1}H NMR (400 MHz, $CHCl_3$, TMS) δ: 0.87(t, J = 6.2 Hz, 3H, Me-5′), 1.12 (s, 3H, Me-13), 1.52 (s, 3H, Me-12), 5.04 (brs, 2H, CH_2-11), 1.74 (m, 1H, H-6a), 2.33 (m, 1H, H-10a), 4.49 (dd, 4.8, 10.8 Hz, 1H, H-8), 6.37 (s, 1H, H-2); ^{13}C NMR (Table 3);

HRESIMS *m/z* 359.1994 [M-H] $^-$ (calcd for $C_{21}H_{27}O_5$, 359.1858).

4.2.16. 1a,4,4-trimethyl-7-pentyl-2,3,4,9c-tetrahydro-1aH-oxireno [2′,3′:3,4]benzo [1,2-c]chromen-9-yl acetate (27)

Following the general experimental conditions, **6** [41] (740 mg, 2.08 mmol) was dissolved in 60 mL of a mixture of hexanes/dichloromethane (1:1) and irradiated for 3 h, 45 min, resulting in the formation of derivative **27** as a resinous matter; $[\alpha]^{26}_D = 4.0$ (*c* 0.10, MeOH); ^{1}H NMR (400 MHz, $CHCl_3$, TMS) δ: 0.88 (t, $J = 6.0$ Hz 3H, Me-5′), 1.28 (s, 3H, Me-12), 1.38 (s, 3H, Me-13), 1.45 (s, 3H, Me-11), 2.30 (s, 3H, Me-15), 3.77 (s, 1H, H-10), 6.47 (s, 1H, H-4), 6.61 (s, 1H, H-2); ^{13}C NMR (Table 3); HRESIMS *m/z* 371.2354 [M+H] $^+$ (calcd for $C_{23}H_{31}O_4$, 371.2222).

4.2.17. 9,10-dihydroxy-6,6,9-trimethyl-3-pentyl-7,8,9,10-tetrahydro-6H-benzo[c]chromen-1-yl acetate (28)

Following the general experimental conditions, **6** (740 mg, 2.08 mmol) was dissolved in 60 mL of a mixture of hexanes/dichloromethane (1:1) and irradiated for 3 h, 45 min, resulting in the formation of derivative **28** (15.7 mg, 2.0%) as a resinous matter; $R_f = 0.40$ (Hexanes- EtOAc, 80:20); $[\alpha]^{26}_D = -9.5$ (*c* 0.21, MeOH); ^{1}H NMR (400 MHz, $CHCl_3$, TMS) δ: 0.86 (t, $J = 6.0$ Hz 3H, Me-5′), 1.20 (s, 3H, Me-12), 1.33 (s, 3H, Me-13), 1.39 (s, 3H, Me-11), 2.13 (s, 3H, Me-15), 4.19 (s, 1H, H-10), 6.25 (brd, 1H, H-2), 6.29 (brd, 1H, H-4); ^{13}C NMR (Table 3); HRESIMS *m/z* 387.2194 [M-H]$^-$ (calcd for $C_{23}H_{31}O_5$, 387.2250).

4.2.18. 9-methoxy-6,6,9-trimethyl-3-pentyl-7,8,9,10-tetrahydro-6H-benzo[c]chromene-1,10-diol (29)

Compound **27** (95 mg, 0.26 mmol) was dissolved in 6.0 mL of MeOH and treated with 180 mg of $NaBH_4$ for 2 1/2 h, diluted with water and extracted with dichloromethane. Removal of solvent and purification on prep TLC afforded **29** (21.8 mg, 23.6%). Treatment of **27** (41 mg, 0.11 mmol) with $NaHCO_3$ (42 mg) in 2 mL of water, MeOH (4 mL), dichloromethane (3 mL) and Adogen® 464 (26 mg), mixed and stirred for 2 h also yielded compound **29** (13 mg, 32.6%) as a resinous matter; $R_f = 0.45$ (Hexanes- EtOAc, 80:20); $[\alpha]^{26}_D = -15.4$ (*c* 0.175, MeOH); ^{1}H NMR (400 MHz, $CHCl_3$, TMS) δ: 0.87 (t, $J = 7.0$ Hz 3H, Me-5′), 1.30 (s, 3H, Me-12), 1.39 (s, 3H, Me-11), 1.49 (s, 3H, Me-13), 2.31 (s, 3H, Me-3″), 3.33 (s, 3H, OMe-1′), 4.26 (s, 1H, H-10), 6.29 (s, 1H, H-2), 6.36 (s, 1H, H-4); ^{13}C NMR (Table 3); HRESIMS *m/z* 385.2479 [M-OH]$^+$ (calcd for $C_{24}H_{33}O_4$, 385.2379).

4.2.19. 10-hydroxy-9-methoxy-6,6,9-trimethyl-3-pentyl-7,8,9,10-tetrahydro-6H-benzo[c]chromen-1-yl acetate (30)

Pd/C (5 mg) was added to a solution of **27** (55 mg, 0.15 mmol) in MeOH. The reaction mixture was stirred while hydrogen was gently bubbled for 10 h, then diluted with water and extracted with dichloromethane. Removal of solvent and purification on prep TLC afforded compound **30** (16 mg, 26.8%); $R_f = 0.46$ (Hexanes- EtOAc, 80:20); $[\alpha]^{26}_D = -17.8$ (*c* 0.09, MeOH); ^{1}H NMR (400 MHz, $CHCl_3$, TMS) δ: 0.87 (t, $J = 7.0$ Hz 3H, Me-5′), 1.22 (s, 3H, Me-12), 1.30 (s, 3H, Me-11), 1.45 (s, 3H, Me-13), 2.31 (s, 3H, Me-3″), 3.32 (s, 3H, OMe-1′), 4.29 (s, 1H, H-10), 6.42 (d, $J = 1.6$ Hz, 1H, H-2), 6.61 (d, $J = 1.6$ Hz, 1H, H-4); ^{13}C NMR (Table 3); HRESIMS *m/z* 385.2479 [M-OH]$^+$ (calcd for $C_{24}H_{33}O_4$, 385.2379).

4.3. Biological evaluation

Anticancer, antimicrobial, antimalarial, and antileishmanial evaluations were conducted in accordance with published procedures [43].

4.3.1. Cell lines and cell culture

4.3.1.1. Cell culture. HEK293 cells (ATCC #CRC-1573) were stably transfected via electroporation with full-length human recombinant cDNA for cannabinoid receptor subtypes 1 and 2 (obtained from Origene). These cells were maintained in a Dulbecco's modified Eagles's medium/F-12 (50/50) nutrient mixture supplemented with 10% fetal bovine serum and either 1% penicillin/streptomycin or 1% G418 sulfate (Geneticin), depending on the cell line. Both cannabinoid cell lines were kept at 37 °C and 5% CO_2. Membranes were prepared by scraping the cells in a 50 mM Tris-HCl buffer, homogenized via sonication, and centrifuged for 40 min at 13650 rpm at 4 °C. The isolated membranes were kept at −80 °C and brought up to room temperature for binding and functional assays. Protein concentration was determined via Bio-Rad protein assay [44].

4.3.2. Radioligand binding for cannabinoid receptor subtypes

In the primary bioassay screen, compounds were tested at a final concentration of 10 μM for competitive binding to the respective receptor. The compounds were added to a 96-well plate followed by 0.6 nM [^{3}H]CP-55,940 and 10 μg of cannabinoid membrane resuspended in 50 mM Tris (pH 7.4), 154 mM NaCl, and 20 mM Di-Na-EDTA supplemented with 0.02% BSA. The cannabinoid assay was incubated at 37 °C for 90 min. The reaction was then terminated by rapid filtration using GF/C (presoaked in 0.3% BSA) and washed with the buffer. Dried filters were then covered with scintillant and measured for the amount of radioligand retained using a Perkin-Elmer Topcount (Perkin-Elmer Life Sciences Inc., Boston, MA, USA). Nonspecific binding, which was determined in the presence of 1 μM CP-55,940 for cannabinoid receptors, was subtracted from the total binding to yield the specific-binding values. Compounds showing competitive inhibition of the labeled ligand to bind to the receptor at 50% or greater were tested in a dose-response curve with concentrations of the test compound ranging from 300 μM to 1.7 nM.

4.4. [^{35}S]-GTP-ϒS binding

For the functional assay, membranes (20μg/well) were incubated with the test compound, 0.5 nM [^{35}S]-GTP-ϒS in 50 mM Tris-HCl, 0.2 mM EGTA, 9 mM $MgCl_2$, 150 mM NaCl, 50 μM GDP, and 1.4 mg ml^{-1} BSA. The reaction was incubated for 2 h at 30 °C and was terminated by rapid vacuum filtration with cold 10 mM Tris-HCl in a Perkin Elmer harvester through GF/B filters. Nonspecific binding was determined by 40 μM of GTP-ϒS.

4.5. Molecular modeling study

4.5.1. Homology modeling

Amino acid sequences of CB_2 was retrieved from the UniProt database (http://www.uniprot.org). Prime [41,45,46] was used for 3D model construction and refinement steps. The models were then validated using BioLuminate suite [27,47–49]. BLAST homology search was run against the non-redundant database of the national center for biotechnology information (NCBI) to identify the highest homologous experimental protein structures from the protein databank (PDB) repository (http://www.rcsb.org). The alignment score of sequence alignment was calculated with the BLOSUM62 similarity matrix (BLOcks Substitution Matrix that is built using sequences with no more than 62% similarity). We used 11.0 for the gap opening cost (penalty) if a gap is introduced in the sequence alignment and 1.0 penalty score for each gap extension. BLAST homology search was carried out for maximum of three iterations at an inclusion threshold of 0.005. The globally conserved residues in the query sequences were examined to aid in selecting the homologous experimental structures.

The crystal structure of CB_1 (PDB accession code: 5XR8 [50]) was

used as the template structure for modeling studies of CB_1. Secondary structure prediction was established by SSPro. We used Prime STA GPCR-specific alignment for sequence alignment and knowledge-based model building method was employed to construct 10 models in each run. We refined the loops using a VSGB solvation model with OPLS 2005 force field and charges. 3D models were then subjected to energy minimization using OPLS2005 force field to remove atomic clashes. The refined models were evaluated by checking the ϕ-ψ angles, chirality, bond lengths, close contacts and also the stereo chemical properties using BioLuminate suite.

4.5.2. Protein preparation

Protein structures were prepared prior to docking by the protein preparation wizard of Schrödinger [51,52]. The original hydrogen atoms were replaced with new ones followed by adjustment of bond orders. Hydrogen bonding network was corrected by adjusting the orientations of the amide groups (Asn and Gln), hydroxyl groups (Tyr, Thr and Ser), and relevant states of imidazole ring (His). The protein structures were then refined by restrained energy minimization using OPLS2005 force field with convergence of heavy atoms to an RMSD of 0.3 Å.

4.5.3. Ligand preparation

Ligands were prepared through LigPrep [53] with OPLS2005 force field and charges with only the lowest energy conformer for each ligand being kept. 2D structures of the compounds were sketched in Maestro and converted into 3D structures to produce corresponding low energy 3D output. Structures were included without performing pre-docking filtering.

4.5.4. Induced fit docking (IFD)

Induced fit Docking (IFD) protocol [54,55] of Schrödinger was used for ligand docking to predict binding modes and associated effects on structural changes of the receptor.

The docking receptor grids were prepared using cavity occupied by the native ligand of CB_1. The CB1 ligand coordinates was copied into the binding pocket of CB_2 to be used in the IFD protocol. Ligand conformational sampling was performed with an energy window of 20.0 kcal/mol. A maximum of 20 poses for each ligand was retained. The poses were required to have a Coulomb-vdW score of <100 and an H-Bond score of <0.05. To attain better binding domain flexibility, Prime Molecular Dynamics module [45] was used to refine all amino residues which fell with 5 Å of each pose. Then, the best 20 poses within 30 kcal/mol were re-docked using Glide [56] SP.

4.5.5. MD simulations

Three MD simulation runs were carried out for CB_1 complexes with compounds **7** and **21**, and CB_2 complex with compound **23**. We used DESMOND _ENREF_48 [57–60]_ENREF_49_ENREF_49 employing OPLS-2005 force field in all MD runs. The proteins were solvated, immersed in membrane (POPC 300K) and energy minimized for 5000 iterations. The minimized structures were subjected to six relaxation steps and protein-ligand contacts were calculated using simulation interactions diagram before the MD production process. The production step was achieved using NPT ensemble. RMSD and RMSF.

Author contribution

AG, SC, ME designed the experiments; AG, AH, WG, MR, DS, SR isolated starting cannabinoids, synthesized and confirmed structures; KE, VY, MK developed computational studies; SK and OD ran enzymatic assays and helped writing the manuscript; PC helped writing, organized and formatted the manuscript.

Acknowledgments

This research was partially funded by the National Institute on drug Abuse (NIDA) contract #N01DA-15-7793. The authors also thank the United States Department of Agriculture, Agriculture Research Service Specific Cooperative Agreement No. 58-6408-7-012, for partial support of this work; Dr. Bharathi Avula for helping with the HRESIFTMS analyses; Dr. Melissa for conducting antimicrobial assays and Dr. Babu Takwani for conducting the anti-leishmanial assay.

Appendix A. Supplementary data

Supplementary data related to this article can be found at https://doi.org/10.1016/j.ejmech.2017.11.043.

References

[1] A.M. Galal, D. Slade, W. Gul, A.T. El-Alfy, D. Ferreira, M.A. Elsohly, Naturally occurring and related synthetic cannabinoids and their potential therapeutic applications, Recent Pat. CNS Drug Discov. 4 (2009) 112–136.
[2] B.J. Cridge, R.J. Rosengren, Critical appraisal of the potential use of cannabinoids in cancer management, Cancer manage. Res. 5 (2013) 301–313.
[3] S. Pisanti, A.M. Malfitano, C. Grimaldi, A. Santoro, P. Gazzerro, C. Laezza, M. Bifulco, Use of cannabinoid receptor agonists in cancer therapy as palliative and curative agents, Best. Pract. Res. Clin. Endocrinol. Metab. 23 (2009) 117–131.
[4] S. Sarfaraz, V.M. Adhami, D.N. Syed, F. Afaq, H. Mukhtar, Cannabinoids for cancer treatment: progress and promise, Cancer Res. 68 (2008) 339–342.
[5] I. Svizenska, P. Dubovy, A. Sulcova, Cannabinoid receptors 1 and 2 (CB1 and CB2), their distribution, ligands and functional involvement in nervous system structures–a short review, Pharmacol. Biochem. Behav. 90 (2008) 501–511.
[6] F.R. Kreitzer, N. Stella, The therapeutic potential of novel cannabinoid receptors, Pharmacol. Ther. 122 (2009) 83–96.
[7] P. Diaz, J. Xu, F. Astruc-Diaz, H.-M. Pan, D.L. Brown, M. Naguib, Design and synthesis of a novel series of N-Alkyl isatin acylhydrazone derivatives that act as selective cannabinoid receptor 2 agonists for the treatment of neuropathic pain, J. Med. Chem. 51 (2008) 4932–4947.
[8] M.P. Davis, Cannabinoids in pain management: CB1, CB2 and non-classic receptor ligands, Expert Opin. Invest. Drugs 23 (2014) 1123–1140.
[9] J. Guindon, A.G. Hohmann, Cannabinoid CB2 receptors: a therapeutic target for the treatment of inflammatory and neuropathic pain, Br. J. Pharmacol. 153 (2008) 319–334.
[10] G.A. Cabral, L. Griffin-Thomas, Emerging role of the cannabinoid receptor CB2 in immune regulation: therapeutic prospects for neuroinflammation, Expert Rev. Mol. Med. 11 (2009) e3.
[11] A.M. Malfitano, C. Laezza, A. D'Alessandro, C. Procaccini, G. Saccomanni, T. Tuccinardi, C. Manera, M. Macchia, G. Matarese, P. Gazzerro, M. Bifulco, Effects on immune cells of a new 1,8-naphthyridin-2-one derivative and its analogues as selective CB2 agonists: implications in multiple sclerosis, PLoS One 8 (2013) e62511.
[12] A. Dhopeshwarkar, K. Mackie, CB2 cannabinoid receptors as a therapeutic target - what does the future hold? Mol. Pharmacol. 86 (2014) 430–437, 438 pp.
[13] A. Kauppinen, T. Nevalainen, M. Hytti, A. Salminen, K. Kaarniranta, T. Parkkari, CB2 receptor as a potential target in age-related diseases, J. Biochem. Pharmacol. Res. 2 (2014) 33–43, 11.
[14] T. Nevalainen, Recent development of CB2 selective and peripheral CB1/CB2 cannabinoid receptor ligands, Curr. Med. Chem. 21 (2014) 187–203.
[15] T. Petrzilka, M. Demuth, Hashish constituents. 7. Synthesis of (-)-11-hydroxy-Δ^8-6a,10a-trans-tetrahydrocannabinol, Helv. Chim. Acta 57 (1974) 121–150.
[16] G. Appendino, S. Gibbons, A. Giana, A. Pagani, G. Grassi, M. Stavri, E. Smith, M.M. Rahman, Antibacterial cannabinoids from cannabis sativa: a structure-activity study, J. Nat. Prod. 71 (2008) 1427–1430.
[17] N.M. Kogan, R. Rabinowitz, P. Levi, D. Gibson, P. Sandor, M. Schlesinger, R. Mechoulam, Synthesis and antitumor activity of quinonoid derivatives of cannabinoids, J. Med. Chem. 47 (2004) 3800–3806.
[18] N.M. Kogan, M. Schlesinger, M. Peters, G. Marincheva, R. Beeri, R. Mechoulam, A cannabinoid anticancer quinone, HU-331, is more potent and less cardiotoxic than doxorubicin: a comparative in vivo study, J. Pharmacol. Exp. Ther. 322 (2007) 646–653.
[19] N.M. Kogan, M. Schlesinger, E. Priel, R. Rabinowitz, E. Berenshtein, M. Chevion, R. Mechoulam, HU-331, a novel cannabinoid-based anticancer topoisomerase II inhibitor, Mol. Cancer Ther. 6 (2007) 173–183.
[20] G. Pryce, C. Visintin, S.V. Ramagopalan, S. Al-Izki, L.E. De Faveri, R.A. Nuamah, C.A. Mein, A. Montpetit, A.J. Hardcastle, G. Kooij, H.E. de Vries, S. Amor, S.A. Thomas, C. Ledent, G. Marsicano, B. Lutz, A.J. Thompson, D.L. Selwood, G. Giovannoni, D. Baker, Control of spasticity in a multiple sclerosis model using central nervous system-excluded CB1 cannabinoid receptor agonists,

FASEB J. 28 (2014) 117–130, 110.1096/fj.1013-239442.
[21] A.S. Husni, C.R. McCurdy, M.M. Radwan, S.A. Ahmed, D. Slade, S.A. Ross, M.A. El Sohly, S.J. Cutler, Evaluation of phytocannabinoids from high-potency Cannabis sativa using in vitro bioassays to determine structure-activity relationships for cannabinoid receptor 1 and cannabinoid receptor 2, Med. Chem. Res. 23 (2014) 4295–4300.
[22] J.W. Huffman, J. Liddle, S. Yu, M.M. Aung, M.E. Abood, J.L. Wiley, B.R. Martin, 3-(1',1'-Dimethylbutyl)-1-deoxy-Δ^8-THC and related compounds: synthesis of selective ligands for the CB2 receptor, Bioorg. Med. Chem. 7 (1999) 2905–2914.
[23] A. Galal, M. Radwan, S. Ahmed, D. Slade, W. Gul, S. Khan, S. Ross, M. ElSohly, Bioactive products from singlet oxygen photooxygenation of Δ^9-THC, Δ^8-THC, and Δ^9-THC-acid-a, Planta medica 78 (2012) 26.
[24] N.M. Kogan, C. Blazquez, L. Alvarez, R. Gallily, M. Schlesinger, M. Guzman, R. Mechoulam, A cannabinoid quinone inhibits angiogenesis by targeting vascular endothelial cells, Mol. Pharmacol. 70 (2006) 51–59.
[25] J.R. Duchek, Preparation of Crystalline Cannabinoid Esters for Cannabinoid Purification, Mallinckrodt Inc, USA, 2004, 22 pp.
[26] C.G. Pitt, M.S. Fowler, S. Sathe, S.C. Srivastava, D.L. Williams, Synthesis of metabolites of delta-9-tetrahydrocannabinol, J. Am. Chem. Soc. 97 (1975) 3798–3802.
[27] A.P. Brogan, L.M. Eubanks, G.F. Koob, T.J. Dickerson, K.D. Janda, Antibody-catalyzed oxidation of delta(9)-tetrahydrocannabinol, J. Am. Chem. Soc. 129 (2007) 3698–3702.
[28] A.T. McPhail, H.N. ElSohly, C.E. Turner, M.A. ElSohly, Stereochemical assignments for the two Enantiomeric pairs of 9,10-dihydroxy-Δ^{6a}(10a)-tetrahydrocannabinols. X-ray crystal structure analysis of (±) trans-cannabitriol, J. Nat. Prod. 47 (1984) 138–142.
[29] A.J. Ganz, P.G. Waser, Testing the pharmacological activity of some synthetic cannabinoids in mice (author's transl), Arzneim 30 (1980) 471–477.
[30] H.H. Wasserman, T.J. Lu, I.A. Scott, The total synthesis of tetracycline, J. Am. Chem. Soc. 108 (1986) 4237–4238.
[31] W. Gul, A. Galal, M.A. ElSohly, P. Carvalho, Crystal structure of (9S,10S)-10-eth-oxy-9-hy-droxy-6,6,9-trimethyl-3-pentyl-7,8,9,10-tetra-hydro-6H-b enzo[c]chromen-1-yl 4-methyl-benzene-sulfonate, Acta Crystallogr. E Crystallogr. Commun. 71 (2015) o1082–1083.
[32] A.J. Ganz, P.G. Waser, Testing the pharmacological activity of some synthetic cannabinoids in mice, Arzneim.-Forsch. 30 (1980) 471–477.
[33] M. Carbone, F. Castelluccio, A. Daniele, A. Sutton, A. Ligresti, V. Di Marzo, M. Gavagnin, Chemical characterization of oxidative degradation products of Δ9-THC, Tetrahedron 66 (2010) 9497–9501.
[34] J.M. Franklin, G.A. Carrasco, Cannabinoid receptor agonists upregulate and enhance serotonin 2A (5-HT(2A)) receptor activity via ERK1/2 signaling, Synapse 67 (2013) 145–159.
[35] J.W. Huffman, S.A. Hepburn, N. Lyutenko, A.L.S. Thompson, J.L. Wiley, D.E. Selley, B.R. Martin, 1-Bromo-3-(1',1'-dimethylalkyl)-1-deoxy-Δ8-tetrahydrocannabinols: new selective ligands for the cannabinoid CB2 receptor, Bioorg. Med. Chem. 18 (2010) 7809–7815.
[36] HPLC, analyzed with a Waters 486 Tunable Absorbance Detector with Semi-Prep Flow Cell, at 350 nm, eluted isocratically with 0.5% anhydrous ethanol in hexanes at a flow rate of 15 mL/min.
[37] M.M. Radwan, M.A. ElSohly, A.T. El-Alfy, S.A. Ahmed, D. Slade, A.S. Husni, S.P. Manly, L. Wilson, S. Seale, S.J. Cutler, S.A. Ross, Isolation and pharmacological evaluation of minor cannabinoids from high-potency cannabis sativa, J. Nat. Prod. 78 (2015) 1271–1276.
[38] M. Elsohly, S. Ross, Method of preparing delta-9-tetrahydrocannabinol - US 20020086438 A1, in, U.S. Patent and Trademark Office - http://www.uspto.gov/, 2002.
[39] Senior Research Scientist in the National Center for Natural Products Research, http://pharmacy.olemiss.edu/ncnpr/team/dr-suman-chandra/.
[40] M. Starks, Marijuana Chemistry: Genetics, Processing & Potency, Ronin Pub, 1990.
[41] R.A. Archer, W.B. Blanchard, W.A. Day, D.W. Johnson, E.R. Lavagnino, C.W. Ryan, J.E. Baldwin, Cannabinoids. 3. Synthetic approaches to 9-ketocannabinoids. Total synthesis of nabilone, J. Org. Chem. 42 (1977) 2277–2284.
[42] D.R. Compton, W.R. Prescott Jr., B.R. Martin, C. Siegel, P.M. Gordon, R.K. Razdan, Synthesis and pharmacological evaluation of ether and related analogues of delta 8-, delta 9-, and delta 9,11-tetrahydrocannabinol, J. Med. Chem. 34 (1991) 3310–3316.
[43] M. Ilias, M.A. Ibrahim, S.I. Khan, M.R. Jacob, B.L. Tekwani, L.A. Walker, V. Samoylenko, Pentacyclic ingamine alkaloids, a new antiplasmodial pharmacophore from the marine sponge Petrosid Ng5 Sp5, Planta medica 78 (2012) 1690–1697.
[44] M.M. Bradford, A rapid and sensitive method for the quantitation of microgram quantities of protein utilizing the principle of protein-dye binding, Anal. Biochem. 72 (1976) 248–254.
[45] M.P. Jacobson, D.L. Pincus, C.S. Rapp, T.J. Day, B. Honig, D.E. Shaw, R.A. Friesner, A hierarchical approach to all-atom protein loop prediction, Proteins Struct. Funct. Bioinforma. 55 (2004) 351–367.
[46] M.P. Jacobson, R.A. Friesner, Z. Xiang, B. Honig, On the role of the crystal environment in determining protein side-chain conformations, J. Mol. Biol. 320 (2002) 597–608.
[47] K. Zhu, T. Day, D. Warshaviak, C. Murrett, R. Friesner, D. Pearlman, Antibody structure determination using a combination of homology modeling, energy-based refinement, and loop prediction, Proteins Struct. Funct. Bioinforma. 82 (2014) 1646–1655.
[48] N.K. Salam, M. Adzhigirey, W. Sherman, D.A. Pearlman, Structure-based approach to the prediction of disulfide bonds in proteins, Protein Eng. Des. Sel. 27 (2014) 365–374.
[49] H. Beard, A. Cholleti, D. Pearlman, W. Sherman, K.A. Loving, Applying physics-based scoring to calculate free energies of binding for single amino acid mutations in protein-protein complexes, PloS one 8 (2013) e82849.
[50] T. Hua, K. Vemuri, S.P. Nikas, R.B. Laprairie, Y. Wu, L. Qu, M. Pu, A. Korde, S. Jiang, J.-H. Ho, G.W. Han, K. Ding, X. Li, H. Liu, M.A. Hanson, S. Zhao, L.M. Bohn, A. Makriyannis, R.C. Stevens, Z.-J. Liu, Crystal structures of agonist-bound human cannabinoid receptor CB1, Nature 547 (2017) 468–471.
[51] G.M. Sastry, M. Adzhigirey, T. Day, R. Annabhimoju, W. Sherman, Protein and ligand preparation: parameters, protocols, and influence on virtual screening enrichments, J. computer-aided Mol. Des. 27 (2013) 221–234.
[52] Schrödinger Suite 2015-3 Protein Preparation Wizard; Epik version 3.3, Schrödinger, LLC, New York, NY, 2015; Impact version 6.8, Schrödinger, LLC, New York, NY, 2015; Prime version 4.1, Schrödinger, LLC, New York, NY, 2015, in.
[53] LigPrep, Version 3.5, Schrödinger, LLC, New York, NY, 2015 (in).
[54] R. Farid, T. Day, R.A. Friesner, R.A. Pearlstein, New insights about HERG blockade obtained from protein modeling, potential energy mapping, and docking studies, Bioorg. Med. Chem. 14 (2006) 3160–3173.
[55] Schrödinger Suite 2015-3 Induced Fit Docking protocol, Glide version 6.8, Schrödinger, LLC, New York, NY, 2015. Prime version 4.1, Schrödinger, LLC, New York, NY, 2015, in.
[56] R.A. Friesner, R.B. Murphy, M.P. Repasky, L.L. Frye, J.R. Greenwood, T.A. Halgren, P.C. Sanschagrin, D.T. Mainz, Extra precision glide: docking and scoring incorporating a model of hydrophobic enclosure for protein-ligand complexes, J. Med. Chem. 49 (2006) 6177–6196.
[57] K.J. Bowers, E. Chow, H. Xu, R.O. Dror, M.P. Eastwood, B.A. Gregersen, J.L. Klepeis, I. Kolossvary, M.A. Moraes, F.D. Sacerdoti, Scalable algorithms for molecular dynamics simulations on commodity clusters, in: SC 2006 Conference, Proceedings of the ACM/IEEE, IEEE, 2006, p. 43.
[58] D. Shivakumar, J. Williams, Y. Wu, W. Damm, J. Shelley, W. Sherman, Prediction of absolute solvation free energies using molecular dynamics free energy perturbation and the OPLS force field, J. Chem. theory Comput. 6 (2010) 1509–1519.
[59] Desmond Molecular Dynamics System, version 4.3, D. E. Shaw Research, New York, NY, 2015. Maestro-Desmond Interoperability Tools, version 4.3, Schrödinger, New York, NY, 2015., in.
[60] Z. Guo, U. Mohanty, J. Noehre, T.K. Sawyer, W. Sherman, G. Krilov, Probing the α-helical structural stability of stapled p53 peptides: molecular dynamics simulations and analysis, Chem. Biol. drug Des. 75 (2010) 348–359.